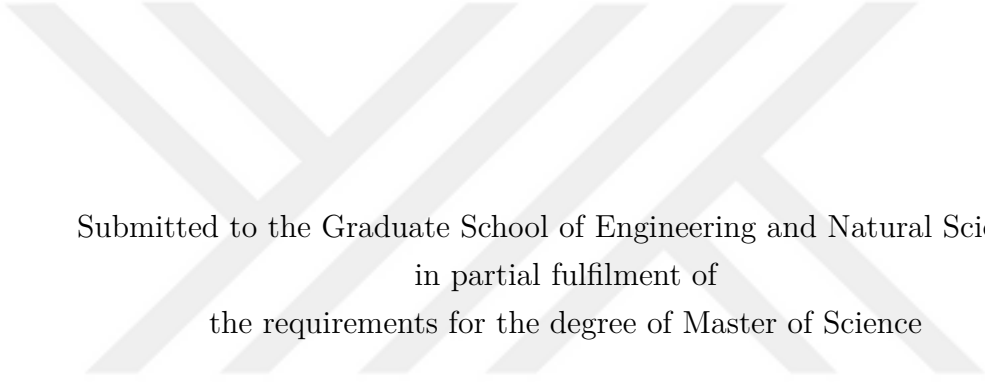


# FULL-BODY MOTION CONTROL OF A HUMANOID ROBOT

by  
ALI FURKAN AKTAŞ



Submitted to the Graduate School of Engineering and Natural Sciences  
in partial fulfilment of  
the requirements for the degree of Master of Science

Sabanci University  
December 2021

# FULL-BODY MOTION CONTROL OF A HUMANOID ROBOT

Approved by:



Date of Approval: Dec 15, 2021



Ali Furkan Aktaş 2021 ©

All Rights Reserved

# ABSTRACT

## FULL-BODY MOTION CONTROL OF A HUMANOID ROBOT

ALI FURKAN AKTAŞ

MECHATRONICS ENGINEERING M.A. THESIS, DECEMBER 2021

Thesis Supervisor: Assoc. Prof. Dr. Kemalettin Erbatur

Keywords: Humanoid, Pushing Control, Parameter Tuning, Ground Force Interaction, Object Force Interaction, Balance Control

Legged systems such as biped robots are more suitable for dynamic tasks to work with humans. Biped robots can achieve better maneuverability and efficiently avoid obstacles because they have better agility and flexibility than other mobile systems like wheeled vehicles. However, the challenges of controlling the biped robots with full-body motion create instability and increase the chance of falling or failure of achieving the tasks.

The thesis presents a method in which the robot maintains balance while pushing the wall in front of it using the reference body reaction forces obtained from the inverse dynamics method. The reference ground reaction forces for both feet are obtained with an optimization technique that uses linear constraints. Calculating the reference ground reaction force allows generating the leg joint torques for the double support phase. Also, a hybrid control method for manipulating arms is introduced to apply the desired pushing force to the wall.

To validate the proposed method, a simulation environment is constructed for the 30-DOF biped robot that includes 3D dynamics and external force reaction models.

## ÖZET

### İNSANSI BİR ROBOTUN TAM VÜCUT HAREKET KONTROLÜ

ALI FURKAN AKTAŞ

MEKATRONİK MÜHENDİSLİĞİ YÜKSEK LİSANS TEZİ, ARALIK 2021

Tez Danışmanı: Doç. Dr. Kemalettin Erbatur

Anahtar Kelimeler: İnsansı Robot, İtme Kontrolü, Parametre Ayarlama, Yer Kuvveti Etkileşimi, Nesne Kuvvet Etkileşimi, Denge Kontrolü

İki ayaklı robotlar gibi ayaklı sistemler, insanlarla çalışmak için dinamik görevler için daha uygundur. İki ayaklı robotlar, tekerlekli araçlar gibi diğer mobil sistemlerden daha iyi çeviklik ve esnekliğe sahip oldukları için daha iyi manevra kabiliyeti elde edebilir ve engellerden verimli bir şekilde kaçınabilir. Bununla birlikte, tam vücut hareketi ile iki ayaklı robotları kontrol etmenin zorlukları, kararsızlık yaratır ve düşme veya görevleri yerine getirmeme şansını artırır.

Tez, ters dinamik yönteminden elde edilen referans vücut reaksiyon kuvvetlerini kullanarak robotun önündeki duvarı iterken dengesini koruduğu bir yöntem sunmaktadır. Her iki ayak için referans zemin reaksiyon kuvvetleri, doğrusal kısıtlamaları kullanan bir optimizasyon tekniği ile elde edilir. Referans zemin tepki kuvvetinin hesaplanması, çift destek fazı için bacak eklemi torklarının oluşturulmasına izin verir. Ayrıca, duvara istenen itme kuvvetini uygulamak için kolların manipüle edilmesi için bir hibrit kontrol yöntemi tanıtılmıştır.

30 serbestlik dereceli iki ayaklı bir robotu, önerilen metot için test etmek amacıyla 3D dinamiklerinin ve dış kuvvetlerinin modellendiği simülasyon ortamı yaratılmıştır.

## ACKNOWLEDGEMENTS

I would like to express my gratitude to everyone who supported and helped me along the way while I was getting my M.Sc.

First of all, I would like to express my gratitude to my advisor, Assoc. Prof. Kemallettin Erbatur, who gave me the chance to work on this thesis, supported me in every aspect, worked very hard, and kept my motivation high throughout this journey.

I would like to express my deep gratitude to my parents, Gülinaz Aktaş and Dinçer Aktaş, who have given me every chance I have had in my life, who have brought me to where I am today, who have always made me feel their endless love and stood by me. Without you, these accomplishments would not have been possible.

Finally, to Gizem Aynur Yılmaz, who was always there for me, did not spare her support even for a moment when I needed it the most.



*To my loving family,  
whom I treasure above everything...*

## TABLE OF CONTENTS

<b>LIST OF TABLES</b> .....	<b>x</b>
<b>LIST OF FIGURES</b> .....	<b>xi</b>
<b>1. INTRODUCTION</b> .....	<b>1</b>
<b>2. Survey on Humanoid Robots</b> .....	<b>3</b>
2.1. History of Biped Robotics .....	3
2.2. Survey Research on Humanoid Balance .....	10
2.2.1. Balance via Position Control .....	10
2.2.2. Balance via Force Control .....	11
<b>3. Dynamics Equations and Framework of the Simulation</b> .....	<b>13</b>
<b>4. Reactive Force Control Scheme</b> .....	<b>18</b>
<b>5. Biped Balance With Reactive Force Control Scheme</b> .....	<b>24</b>
5.1. Reaching the Wall .....	26
5.2. Maintaining Balance While Pushing .....	29
5.2.1. Generate Body Reference Reaction Forces .....	29
5.2.1.1. First Case .....	29
5.2.1.2. Second Case .....	30
5.2.2. Generate Leg Joint Torques Via Body Reference Reaction Force	31
5.2.3. Arm Hybrid Control and Generation of Generalized Joint Torques .....	31
5.3. A Simple technique for Comparison Purposes .....	32
5.4. Block Diagrams .....	33
<b>6. Simulation Results</b> .....	<b>36</b>
6.1. Robot Arm Manipulation Via Position Control .....	37
6.2. Generation of Ground Reaction Forces .....	38
6.3. On Robot Arm Control via Hybrid Control .....	45

<b>7. Conclusion .....</b>	<b>46</b>
<b>BIBLIOGRAPHY.....</b>	<b>47</b>



## LIST OF TABLES

Table 5.1. Dimensions and weight data of SURALP .....	25
---	----



## LIST OF FIGURES

Figure 2.1. Waseda University’s first humanoid robots (Takanishi, 2019) ..	3
Figure 2.2. WABIAN-RII (left) and WABIAN-RIV (right) (Yu Ogura, Aikawa, Shimomura, Kondo, Morishima, Hun-ok Lim & Takanishi, 2006) and (Lim & Takanishi, 2007).....	4
Figure 2.3. HONDA’s humanoid robot family includes the following models: E0-6, P1-3, and ASIMO (Yampolskiy & Gavrilova, 2012).....	5
Figure 2.4. HRP-2 (left), HRP-3 (middle) and HRP-4 (right) (Kaneko, Kanehiro, Kajita, Hirukawa, Kawasaki, Hirata, Akachi & Isozumi, 2004),(Kaneko, Harada, Kanehiro, Miyamori & Akachi, 2008a) and (Kaneko, Kanehiro, Morisawa, Akachi, Miyamori, Hayashi & Kanehira, 2011) .....	6
Figure 2.5. CB humanoid robot of SARCOS (Morimoto, Atkeson, Endo & Cheng, 2007) .....	7
Figure 2.6. PETProto (left) and PETMAN (right) (Nelson, Saunders & Playter, 2019) .....	8
Figure 2.7. AtlasProto (left) and Atlas (right) (Nelson et al., 2019) .....	9
Figure 4.1. For small angles, definition of orientation error .....	20
Figure 4.2. Contact Points of the foot.....	21
Figure 4.3. The matrix $\mathbf{K}'$ establishes a relationship between the reactive force and torque given to the robot’s body and the ground contact forces at the robot’s foot corners. ....	23
Figure 5.1. The kinematic arrangement of SURALP .....	24
Figure 5.2. SURALP’s coordinate systems. $o_w$ and $o_b$ denote the world’s origins and body coordinate frames, respectively. ....	25

Figure 5.3. Snapshots from the OpenGL based animation window. Robot initial configuration (left) and the configuration at the wall contact instant with hands moved forward (right). Initial conditions of the hands are 0.235 m in the world coordinate frame. The wall is not shown in animation. It is placed at 0.3 m parallel to the world frame y-z plane. Two snapshots above described the robot motion before the wall contact. ....	27
Figure 5.4. The block diagram of the simple independent joint position control based technique .....	33
Figure 5.5. Reactive Force Control Case 1. Body is aimed to be kept at its original posture via reactive force control. Hybrid control is implemented for the arms. ....	34
Figure 5.6. Reactive Force Control Case 2. Body receives a feed-forward wall contact force when hand touched the wall. ....	35
Figure 6.1. Snapshots from the OpenGL based animation window. Robot initial configuration (left) and the configuration when hands moved forward to 0.4 m in the body coordinate frame(right). Hand keep the contact with wall and push the body away from it. The wall is not shown in animation. It is placed at 0.3 m parallel to the world frame y-z plane. The initial configuration is picture is the same as in Figure 5.3 and is given here in order to compare initial and final configurations side by side. Note that in the right hand side picture, the arms are extended to 0.4 m in the x-direction where as the right hand side picture of Figure 5.3 shows hands stopped at 0.3 m, at the wall.....	36
Figure 6.2. Arm joint position error during reaching the wall.....	37
Figure 6.3. Ground reaction forces at contact points in z-axis for Case 1 ..	39
Figure 6.4. Position of the base for Case 1 .....	39
Figure 6.5. Position of the center of pressure for Case 1 .....	40
Figure 6.6. Robot initial posture (left), robot applies 94 N per hand (right) at the wall successfully. The initial posture is not different from the ones in Figures 5.3 and 6.1. It is shown here for a side by side comparison with the final configuration. Case 1 of reactive control: Body posture kept essentially at the initial condition in contrast to the basic position control case shown in Figure 6.1. ....	40
Figure 6.7. Ground reaction forces at contact points in z-axis for Case 2, applied force is 90 N .....	41
Figure 6.8. Position of the base for case 2, applied force is 90 N.....	42

Figure 6.9. Position of the center of pressure for Case 2, applied force is 90 N .....	42
Figure 6.10. Ground reaction forces at contact points in z-axis for Case 2, applied force is 117 N.....	43
Figure 6.11. Position of the center of pressure for Case 2, applied force is 117 N .....	43
Figure 6.12. Snapshots from the OpenGL based animation window. Robot initial configuration (left) and the configuration in the steady state (right). The left hand side picture is not different from the initial posture pictures in Figures 5.3, 6.1 and 6.6. It is shown here for a side by side comparison with the final configuration on the right. Case 2 of reactive control. The wall is not shown in animation. It is placed at 0.3 m parallel to the world frame y-z plane. A comparison of the right hand side picture in this figure with the right hand side picture with in Figure 6.6 (Case 1 of Reactive Control) shows that the robot body moves slightly closer to the wall with Case 2. The wall contact force reference is used in a feed-forward fashion for the body control force reference and this reference created the leaning-on-the-wall effect shown in the picture.....	44
Figure 6.13. Arm endpoint positions for Case 2, applied force is 117 N .....	45

## 1. INTRODUCTION

The number of research projects has increased on humanoid robots for the past four decades. The fundamental objective of designing humanoids is to cooperate with humans in the work environment. Biped robots are more suitable than other mobile robots for complicated application situations, e.g., disaster rescue or exploration. Full-body motion control with hands and feet in contact with the environment is a significant area of research because a humanoid should preserve its balance while completing a task, i.e., manipulating an object or walking on uneven terrain (Harada, Kajita, Kaneko & Hirukawa, 2003).

The non-linear and complex structure of a humanoid (Vukobratović, Borovac, Surla & Stokić, 1990) makes the control of biped robots with stability while interacting with the environment an appealing topic to explore. There is extensive research on humanoid walking, adapting external disturbances, achieving tasks e.g., opening doors, climbing ladders, manipulating objects. Model Predictive Control (Wieber, 2006) is a generic control strategy designed to deal with constrained dynamical systems. The Capture Point method (Englsberger, Ott, Roa, Albu-Schäffer & Hirzinger, 2011) is also using Linear Inverted Pendulum Model (LIPM) and with tracking of the "extrapolated center of mass". The Passivity-based controller (Hyon, Hale & Cheng, 2007) distributes the desired force that is applied to the ground to the predefined contact points and transforms it directly to the joint torques.

It is envisioned that humanoid robots will co-exist with humans in industrial working frameworks. Application of a predefined force on the environment is one of the typical actions of a human worker. This can be for an assembly task, a drilling operation, moving a wheeled cart or pushing a large object on a horizontal surface to change its position. Pushing large object is addressed in (Harada, Kajita, Kanehiro, Fujiwara, Kaneko, Yokoi & Hirukawa, 2007) also mentioned above. However, in many applications, the worker should keep his/her feet at a fix location and apply force by hands without losing balance. Exploring limits of pushing force in such a condition and designing control approaches for increasing pushing force capacity are significant for these kind of applications when a humanoid robot replaces the human

worker. With this motivation, this thesis focuses on applying a pushing force on a wall while preserving a desired posture and foot locations of the robot. As mentioned above, although there are full-body motion control studies reported in the literature on humanoid robots, this specific significant problem is not investigated directly. For this problem, this thesis proposes two solutions via the use of ground reaction forces.

The robot will maintain balance when Center of Pressure (CoP) is inside the convex hull of the foot-supporting region; however, when the applied pushing force increases, CoP shifts to the edge of this region, and the robot falls backward. Thus, hand reaction forces must be compensated so that robot stays in balance. In the proposed method, a force control is implemented to preserve the robot's desired foot positions. The body of a humanoid robot is not actuated directly, but ground reaction forces determine the body dynamics. Therefore, ground reaction forces are generated for this hybrid control scheme. The generation of reference reaction forces is obtained with an optimization technique that uses linear constraints of supporting legs. Thus, desired ground reaction forces of the supporting legs' predefined contact points can be directly transformed to the suitable leg joint torques. Additionally, a hybrid of position and force control is employed for the arms to ensure that contact points are fixed when pushing and the desired force is applied to the wall. Two main approaches proposed and compared. The first one, referred to as Case 1, tries to stabilize the robot body in a fixed configuration while pushing the wall and the second one, Case 2, pushes the body towards to wall via ground reaction forces to create a leaning-on-the-wall effect.

The full-body control and balance tests are conducted in the SURALP (Sabanci University Robotics ReseArch Laboratory Platform) simulation environment for humanoid robots, which was developed at Sabanci University in the framework of a project funded by TUBITAK (The Scientific and Technological Research Council of Turkey).

The next chapter presents a literature review on the history of biped robots and approaches for maintaining balance. Chapter 3 describes the biped model employed in this study, the framework for the simulation equations. The reactive force control scheme for a biped robot with dynamics of body and legs is discussed in Chapter 4. Chapter 5 presents how the reactive force control scheme and proposed reactive force control methods are used when the biped is applying force on the wall. The two methods, Case 1 and Case2, are compared. Simulation results are given in Chapter 6. The final chapter highlights the research work carried out and the conclusions are drawn. The section also suggests future research directions.

## 2. Survey on Humanoid Robots

### 2.1 History of Biped Robotics

Researchers' interest in humanoid robotics grew in the late 1960s, producing many experimental robots. During this time, Professor Ichiro Kato, a pioneer in robotics, began researching human mobility and, in 1967, at Waseda University, built the WL-1 artificial lower-limb biped walker (Lim & Takanishi, 2007). Fundamental bipedal locomotion analysis began with this foundation (Figure 2.1). After the WL-3 and WL-5 prototypes, the world's first full-scale humanoid robot, WABOT-1, was built in 1973. This robot could walk straight, change directions while walking, and interact with the environment by calculating distances and conversing Japanese with artificial external senses. Takanishi et al. demonstrated dynamic walking for the first time in 1984, using torque input from torque sensors mounted to the ankle and hip joints (Takanishi, Ishida, Yamazaki & Kato, 1985), after experiments on quasi-dynamic walking with the WL-9DR and planar walking with the WL-10R. These studies proceeded with the WL-12 series of hydraulic biped robots and prototypes WL-15 and WL-16.

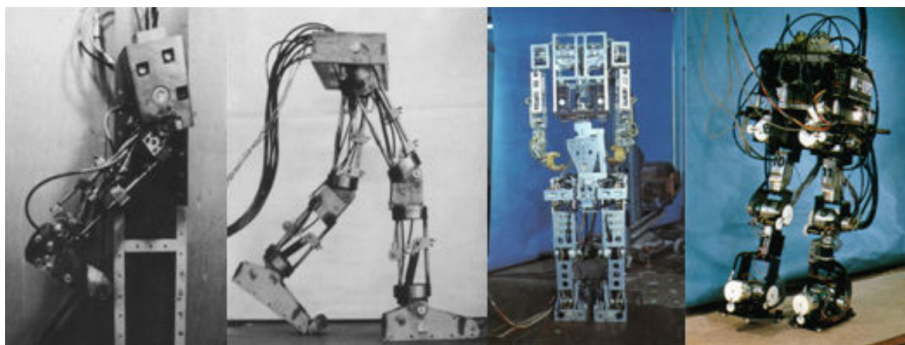


Figure 2.1 Waseda University's first humanoid robots (Takanishi, 2019)

in 1996, WABIAN (**W**Aseda **B**Iped **H**um**A**Noid robot) was produced to develop a human-sized robot with 35 degrees of freedom that is driven by electric motors and walks at the same speed as a person. WABIAN-RII was launched in 1999 as a result of research on robot-environment interaction accomplished with this prototype (Lim & Takanishi, 2000). The WABIAN-RIV was introduced in 2004 following the development of the WABIAN-RIII prototype to absorb shock on foot landing. In order to mimic some of the human senses, it employs visual and voice recognition algorithms. WABIAN- RIV stands 1.89 m tall and weighs 127 kg. He is 43 D.O.F.(Figure 2.2).

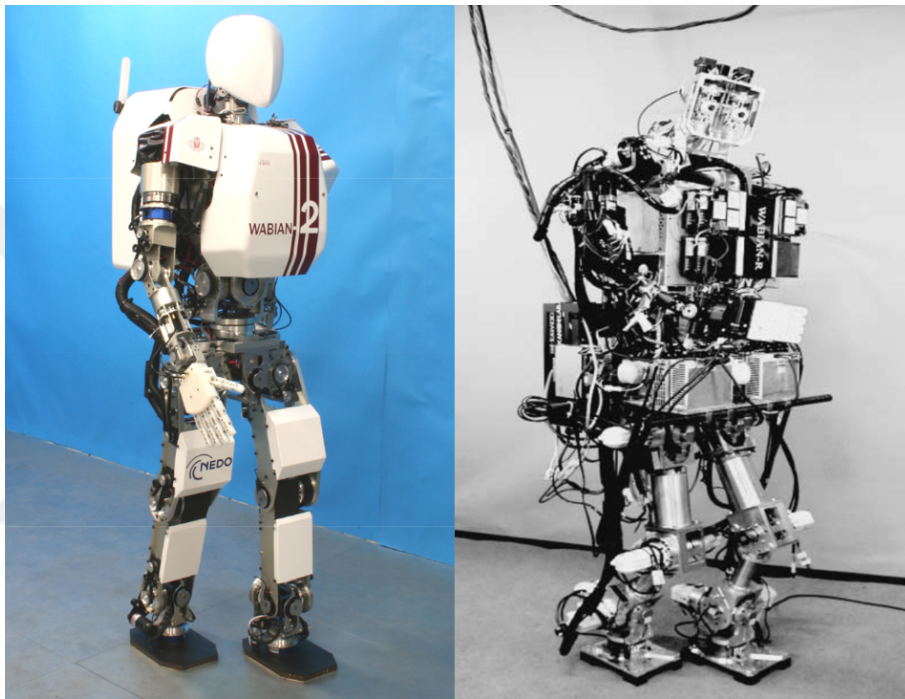


Figure 2.2 WABIAN-RII (left) and WABIAN-RIV (right) (Yu Ogura et al., 2006) and (Lim & Takanishi, 2007)

Since 1986, HONDA has played a vital role in humanoid robotics research and attracted global interest by inventing the most intriguing humanoid robots (Figure 2.3). The principles of bipedal walking are investigated with the early prototypes E0, E1, E2 (which enables the first dynamic walking), and E3, and the stability of the walking is further enhanced with the employment of posture balancing control methods with the subsequent prototypes E4, E5, and E6. After constructing the first humanoid model P1, in 1996, the public was introduced to the following prototype P2, which is referred to as the world's first autonomous walking humanoid robot using wireless technology. P2 was able to move freely, climb and descend stairs, and do numerous manipulation tasks without the need of wires. Following this outstanding achievement, the subsequent prototype, P3, concentrated on increasing the

robot's dependability and improving the robot's size and weight for human use. As a consequence of this downsizing and the conversion from aluminum to magnesium construction material, the robot's height is decreased from 1.82 m to 1.6 m and its weight is reduced from 210 kg to 130 kg.



Figure 2.3 HONDA's humanoid robot family includes the following models: E0-6, P1-3, and ASIMO (Yampolskiy & Gavrilova, 2012)

In 2000, following the success of P2 and P3, the last humanoid robot ASIMO (**A**dvanced **S**tep in **I**nnovative **M**Obility) is launched. This robot's look and movement were more human-like than those of prior versions. This robot stands 1.2 meters tall and weighs 43 kilograms. It is capable of performing a variety of tasks in a human-inhabited environment because of its better locomotion and arm operating capabilities, and a compact and lightweight structure. By utilizing a revolutionary walking technology called i-WALK, ASIMO is capable of continuous walking and running while changing directions and interacting with its surroundings (Hirai, Hirose, Haikawa & Takenaka, 1998).

The Japanese Ministry of Economy and Industry founded the Humanoid Robot Project (HRP) in 1998 to research and build humanoid robot capable of performing physical activities in the workplace. Honda Research and Development created the HRP-1 prototype to improve upon the Honda P-3 prototype, featuring the controller system (Hirukawa, 2007). The prototype is 1.6 meters tall and 120 kilos in weight, made up of 30 D.O.F. The National Institute of Advanced Industrial Science and Technology (AIST) created the HRP-1S control system in 2001, allowing simultaneous control of both arms and legs. This prototype is used in industrial vehicle teleoperation and patient care. HRP-2, the project's second platform, began with the leg module HRP-2L, the arm module HRP-2A, and a prototype HRP-2P. The enhancement of these modules culminated in the launch of HRP-2, which has a

smaller (1.54 m and 58 kg) and lighter (1.54 m and 58 kg) body without a backpack. This robot is often used in humanoid robotics research and development. HRP-3, the subsequent prototype from AIST, included a waterproof mechanical and electrical structure. This structure allows work to be conducted in inclement weather and open areas. Additionally, HRP-3 was equipped with revised hand and wrist designs to enhance the handling and functionality of previous prototypes (Kaneko, Harada, Kanehiro, Miyamori & Akachi, 2008b). The prototype humanoid robots HRP-2 and HRP-3 are seen in (Figure 2.4). AIST's most current humanoid robot prototype, HRP-4, debuted in 2009, is equally lightweight and seems to have a slim physique. These humanoid robots are designed to maintain equipment, guard homes, and businesses, drive industrial vehicles, assist the elderly, and interact with humans in work environments (Hirukawa, 2007).



Figure 2.4 HRP-2 (left), HRP-3 (middle) and HRP-4 (right) (Kaneko et al., 2004),(Kaneko et al., 2008a) and (Kaneko et al., 2011)

Another example of humanoid robots is the SARCOS Company's CB (Computational Brain) systems. These prototypes for SARCOS's humanoid robot project were conceived and manufactured to simulate human movements and computational brain operations. JST (Japan Science and Technology Agency), ICORP Computational Brain Project, and ATR Computational Neuroscience Laboratories collaborate on this project. The CB prototype is a bipedal humanoid robot that weighs 92 kg and stands 1.575 m tall (Cheng, Hyon, Morimoto, Ude, Colvin, Scroggin & Jacobsen, 2006). (Figure 2.5). The experimental experiments conducted in this project attempt to comprehend the biological facts behind bipedal walking and develop control algorithms based on computational brain processes. The project's primary objectives are to maintain a steady bipedal walk, stabilize balance, and govern physical

contact. Techniques for compensating for gravity enable the robot to adapt and respond to external forces. In addition, force control algorithms are used to achieve full-body equilibrium.

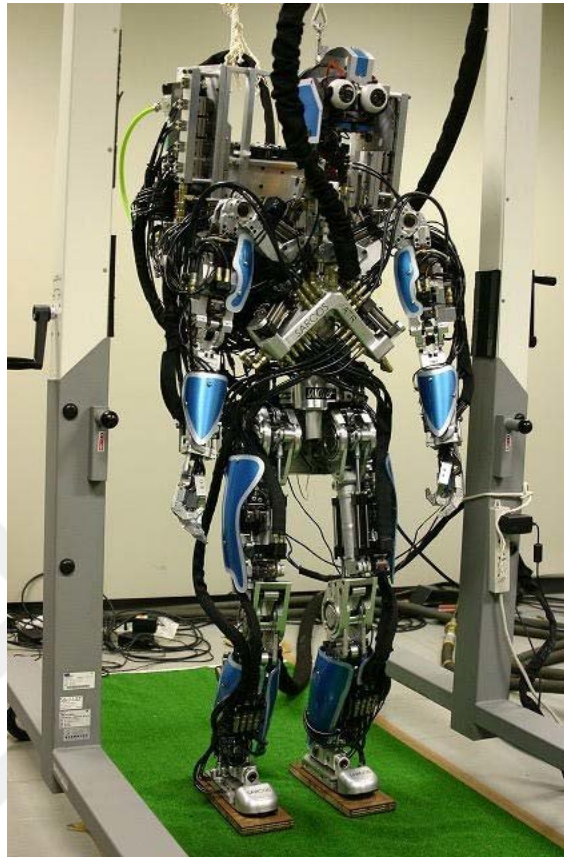


Figure 2.5 CB humanoid robot of SARCOS (Morimoto et al., 2007)

Boston Dynamics started construction of PETMAN, a humanoid robot designed to test chemical protection equipment for the Army, in December 2008 (Nelson, Saunders, Neville, Swilling, Bondaryk, Billings, Lee, Playter & Raibert, 2012). PETMAN was developed as a robotic human proxy to test chemical protective equipment. The robot was intended to wear protective clothes while walking and performing basic activities in a controlled environment. Chemical sensors placed in the robot's skin monitor the presence, timing, and location of chemical agents inside the suit. Since a fundamental necessity for the PETMAN robot was to execute natural human-like actions, walking gait, in 2009, Boston Dynamics introduced the PETMAN Prototype (PETProto) as the company's first biped to continue developing novel walking gaits. PETProto had two five-degree-of-freedom legs, with the most focus on hip abduction/adduction, and displayed a dynamic, high-speed walking gait with the remaining degrees of freedom devoted to sagittal plane limb movement. PETProto stood roughly 1.5 meters tall, with hips around 1 meter above the ground (Figure 2.6).

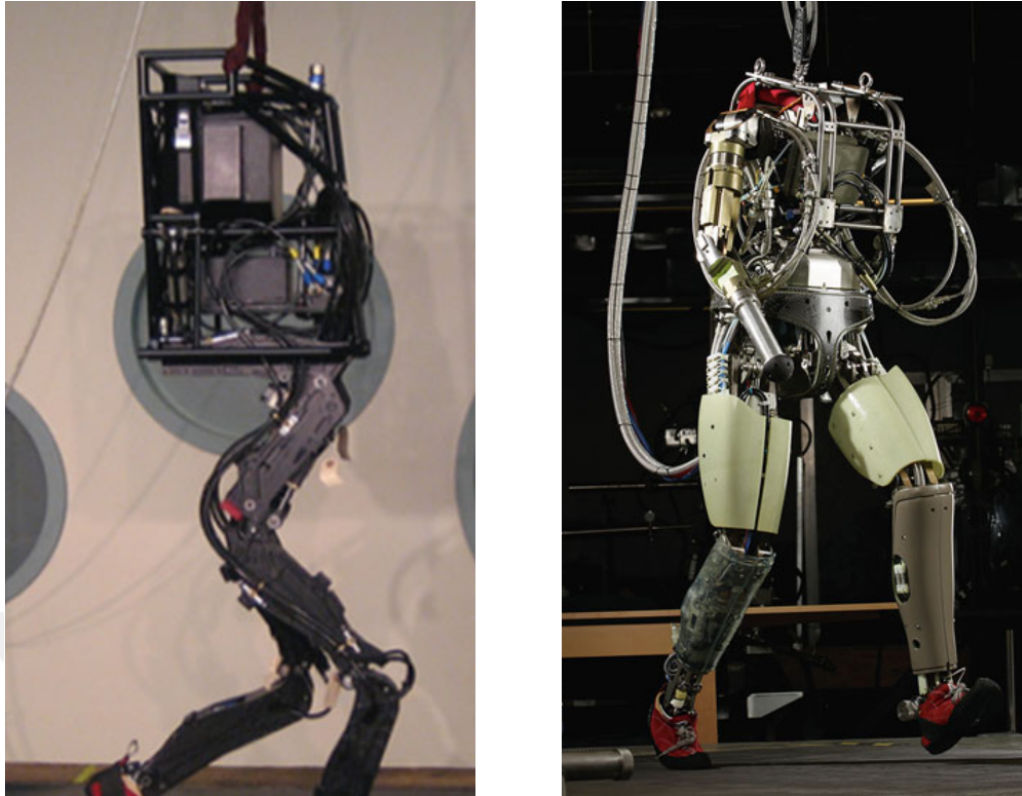


Figure 2.6 PETProto (left) and PETMAN (right) (Nelson et al., 2019)

PETMAN was developed in 2011 to be the size of a 50th percentile human and to move in a manner similar to that of a human, including a natural walking gait. (Figure 2.6). PETMAN was a self-propelled biped powered by an off-board hydraulic power unit (HPU). Inertial sensors monitor the body's attitude and acceleration, while joint sensors measure the actuators' motion and force. PETMAN's position in space was estimated using input from these sensors by the on board computer. Additional off-board sensors in the HPU were used to monitor PETMAN's balance: hydraulic pressure, flow, and temperature. The robot had 29 actuated DoF, weighed around 108 kg, and stood approximately 170 cm tall.

AtlasProto (Figure 2.7) as produced by simply equipping PETProto with arms. Each arm had a two-degree-of-freedom shoulder, a one-degree-of-freedom elbow, a passive spring-loaded prismatic forearm joint, and a basic hemispherical "hand." AtlasProto recognized when the hand made contact with the environment and amount of force was created axially down the forearm due to the springs and sensors in the forearm joint. Researchers added two new goals to the biped work with AtlasProto: dynamic stair climbing and navigating a simulated catastrophe corridor filled with large objects. These activities required the robot to balance by supporting with its arms. One critical component of the dynamic stair ascent was balancing the sagittal plane through foot placing time.

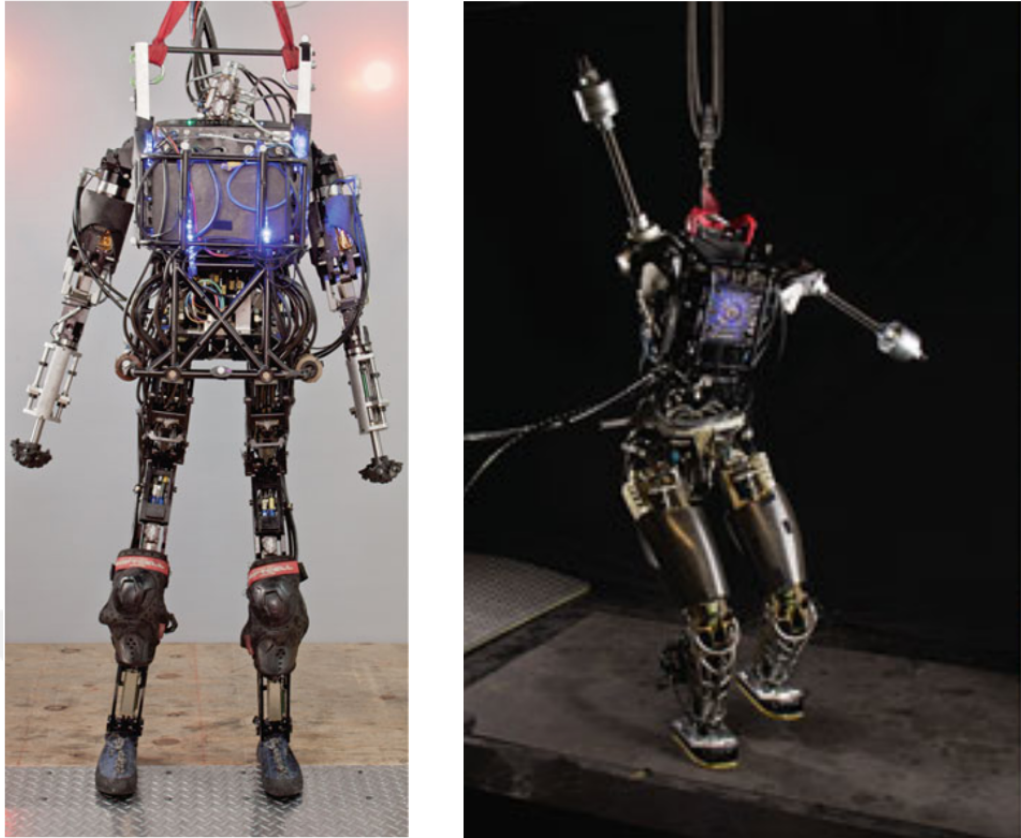


Figure 2.7 AtlasProto (left) and Atlas (right) (Nelson et al., 2019)

Atlas (Figure 2.7) is constructed with PETMAN's lower body, a simplified torso, movable shoulders, and club-like arms. The arms assisted in the control of angular momentum. The most significant control-enabling hardware improvement made in Atlas was the addition of CoP sensors on the feet, which enabled active closed-loop CoP regulation, providing Atlas with far superior standing stability than PETMAN. Atlas was first created for walking over uneven and inclined terrain with reactive foot placement control and building the first suitable balance controller with better state estimation and angular momentum. The balancing controller was later enhanced with the "Capture Point" algorithm. The Capture Point enables the walking controller to link the dynamics of the center of mass (CoM) in lateral and sagittal orientations to ground contact forces. As a result, the system evolved into a more general one for locomotion tasks involving precise foot location, such as climbing stairs, avoiding obstacles, or reaching an object to operate (Nelson et al., 2019).

## 2.2 Survey Research on Humanoid Balance

The challenges of controlling the biped robots with full-body motion create instability and increase the chance of falling or failure of achieving the tasks. The contact between the foot of the biped robot and the ground creates a passive DOF (Vukobratović & Borovac, 2005). In addition, because of the nature of the walking, a biped robot has two different phases throughout with gait cycle and ground contact. In the single support phase, the number of equations is higher than the unknown variables and during the double support phase. The biped robot is under-actuated in the single-support phase while turning into an over-actuated system in the double-support phase (Chevallereau, Bessonnet, Abba & Aoustin, 2009). In addition, during the exchange of these phases, there are impact forces to the robot from the ground. For walking humanoids, the fundamental goal of control is to maintain dynamic balance by ensuring a proper ground reaction force and adapting to unknown external forces (Ott, Roa & Hirzinger, 2011).

### 2.2.1 Balance via Position Control

With a high-performance balancing controller, humanoid motion planning becomes more stable and flexible; thus, a balancing controller becomes a critical component in the development of humanoid robots. Additionally, whole-body synchronization cannot be achieved without using a balance controller.

The first balancing criterion is the position of the humanoid robot's center of mass (COM) and center of pressure (COP). If the COM or COP of a robot is constrained inside the convex hull of the foot support region, the robot is considered stable (Feng, Xinjilefu, Atkeson & Kim, 2016). The ZMP is the second criteria, which is a position on the ground where the tangential components of the moment created by the ground reaction force/moment become zero. Thus, the robot will keep its balance when the position of ZMP is inside the convex hull of the foot-supporting area (Harada et al., 2003). At the core of the concept, several research topics for humanoid robots include walking pattern generation (Kajita, Kanehiro, Kaneko, Fujiwara, Yokoi & Hirukawa, 2002), walking and running control (Nagasaki, Kajita, Yokoi, Kaneko & Tanie, 2003), balancing control (Stephens & Atkeson, 2010), dual-arm manipulation, and whole-body coordination (Sentis & Khatib, 2005). The linear inverted pendulum

model (LIPM) provides a straightforward mathematical representation of a bipedal walking robot. Unlike a standard inverted pendulum, it has linear dynamics, which helps understand walking dynamics, designing biped gaits, and developing biped controllers, but it only examines three position variables on a humanoid robot's center of mass. Preview Control (Kajita, Kanehiro, Kaneko, Fujiwara, Harada, Yokoi & Hirukawa, 2003) is one of the methods that use LIPM for walking pattern generation. The humanoid robot's centroidal angular momentum can be controlled thanks to the installation of a flywheel, and the capture point presented in (Pratt, Carff, Drakunov & Goswami, 2006). The Capture Point method is also using LIPM, and with tracking of the capture point, which can be defined as the "extrapolated center of mass" as in (Hof, 2008), stable walking can be achieved, and also it proposes a new balancing controller to adapt external disturbances (Englsberger et al., 2011). Model Predictive Control (Wieber, 2006), also can be defined as "Receding Horizon Control", is a generic control strategy designed to deal with constrained dynamical systems and have the capability to react large range of situations. This method is also an improvement of the ZMP Preview Control scheme.

### 2.2.2 Balance via Force Control

Newton's principles state that any form of locomotion, including legged locomotion, is based on the application of interaction forces to the environment in order to advance the system and, hence, its total center of mass (CoM). There are multiple stance phases throughout with gait cycle and ground contact in legged locomotion. The total applied contact force controls how the CoM will move during each stance phase. Thus, balance control, which aims to maintain the CoM's stability against external disturbances, can be achieved through the control of CoM via contact forces. This concept is feasible for small and medium-sized disturbances due to the control of contact forces and the use of angular momentum changes generated by whole-body motion. For more serious disturbances, stability of the CoM necessitates change of the contact points. Balance is directly associated with environmental interaction forces because these forces are the only source of the robot to counter gravity and provide acceleration towards the goal. However, the friction cone and other constraints on environmental interaction forces make it difficult to maintain balance. Three characteristics must be considered for direct control of interaction forces. First, interactions between several contact points of interest must be controlled. Second, the controller must adapt compliantly to arbitrary unknown external pressures to avoid interfering with the first aspect. Thirdly, the

controller should not violate constraints such as the unilaterality of some contact forces, friction, zero moment point (ZMP), or pressure center (CoP).

Suppose the first aspect, as mentioned above, is the only objective for the controller. In that case, force tracking can be performed by measuring the interaction forces (applied to the feet or hands) to calculate the joint angle deviation to decrease force tracking errors. The mentioned method is referred to as position-based force control. Due to the difficulty of addressing the second aspect, as mentioned above, several researchers have developed direct force control strategies for manipulators based on their dynamics in addition to their kinematics (Khatib, 1987). These investigations also led to the development of redundancy resolution techniques. The first work that considers the third aspect and covers the ground response force control as a constrained nonlinear optimization problem is (Fujimoto & Kawamura, 1998).

(Pratt, Chew, Torres, Dilworth & Pratt, 2001) is the first publication to discuss the implementation of balance control using torque-controlled actuators wherein virtual model control was applied to a planar biped robot. Researchers presented and implemented explicit contact force optimization on a full-sized torque-controlled humanoid robot using a passivity-based redundant resolution control system (Hyon et al., 2007). The Passivity-based controller distributes the desired force that is applied to the ground to the predefined contact points and transforms it directly to the joint torques while manipulating objects or adapting to an unknown environment. This method does not require contact force measurement or inverse kinematics or dynamics. The same approach is also presented to adaption to uneven terrains in (Hyon, 2009). By distributing the balancing pressures to predefined contact points, the posture and balance control approach suggested in (Ott et al., 2011) adjusts to unforeseen environmental disturbances. The technique is based on the notion that grasping an item and balancing a robot are essentially similar in that both require trying to achieve the desired wrench via the application of sufficient forces at the contact points.

### 3. Dynamics Equations and Framework of the Simulation

Base-link position and orientation dynamics must be characterized as a free-fall manipulator, similar to the biped robot characterisation, that interacts with but is not attached to the environment. Let  $\mathbf{x}$ ,  $\mathbf{v}$ ,  $\mathbf{u}$  represent generalized coordinates, velocity, and force, respectively.

$$\mathbf{x}^T = [\mathbf{p}_B^T, \mathbf{A}_B^T, \boldsymbol{\theta}^T] \in R^3 \times SO(3) \times R^N \quad (3.1)$$

$$\mathbf{v}^T = [\mathbf{v}_B^T, \mathbf{w}_B^T, \mathbf{w}^T] \in R^3 \times R^3 \times R^N \quad (3.2)$$

$$\mathbf{u}^T = [\mathbf{f}_B^T, \mathbf{n}_B^T, \boldsymbol{\tau}^T] \in R^3 \times R^3 \times R^N \quad (3.3)$$

where

$\mathbf{p}_B$  :  $3 \times 1$  vector representing position of the base-link

$\mathbf{A}_B$  :  $3 \times 3$  matrix representing attitude of the base-link

$\boldsymbol{\theta}$  :  $N \times 1$  vector representing the joint angle

$\mathbf{v}_B$  :  $3 \times 1$  vector representing the base-link velocity

$\mathbf{w}_B$  :  $3 \times 1$  vector representing the angular velocity of base-link

$\mathbf{w}$  :  $N \times 1$  vector representing the joint angular velocity

$\mathbf{f}_B$  :  $3 \times 1$  vector representing the generated force in base-link

$\mathbf{n}_B$  :  $3 \times 1$  vector representing the generated torque in base-link

$\mathbf{n}_B$  :  $3 \times 1$  vector representing the generated torque by actuator

$\mathbf{n}_B$  :  $3 \times 1$  torque vector representing the generated by actuator

$N$  : The robot's number of joints

The transformation matrix  $\mathbf{A}_B$  defines the relationship between the link axes and the world axes. The robot's motion equations are as follows:

$$\dot{\mathbf{p}}_B = \mathbf{v}_B \quad (3.4)$$

$$\dot{\mathbf{A}}_B = \mathbf{w}_B \times \mathbf{A}_B \quad (3.5)$$

$$\dot{\boldsymbol{\theta}}_B = \mathbf{w} \quad (3.6)$$

and

$$\mathbf{H}(\mathbf{x})\dot{\mathbf{v}} + \mathbf{C}(\mathbf{x}, \mathbf{v})\mathbf{v} + \mathbf{g}(\mathbf{x}) = \mathbf{u} + \mathbf{u}_E \quad (3.7)$$

where

$\mathbf{H}(\mathbf{x})$  :  $(N+6) \times (N+6)$  inertia matrix

$\mathbf{C}(\mathbf{x}, \mathbf{v})$  :  $(N+6) \times (N+6)$  matrix representing centrifugal and Coriolis effects

$\mathbf{g}(\mathbf{x})$  :  $(N+6) \times 1$  vector representing gravity effect

$\mathbf{u}_E$  :  $(N+6) \times 1$  vector representing generalized forces generated by external forces

The biped robot is represented using Equation (3.7), which provides the general form of the dynamic equation. A simulation environment is employed using the actuator torque input to evaluate the proposed method of numerically computing the angles of the joints and the position of the body at each step-time. The following definitions describe the procedure for simulating the biped system. At each step time  $h$ , Euler integration updates the generalized states  $(\mathbf{x}, \mathbf{v})$ .

$$\mathbf{p}_B(t+h) = \mathbf{p}_B(t) + h\mathbf{v}_B(t) \quad (3.8)$$

$$\mathbf{A}_B(t+h) = \mathbf{T}(h\mathbf{w}_B)\mathbf{A}_B(t) \quad (3.9)$$

$$\theta(t+h) = \theta(t) + h\omega \quad (3.10)$$

$$\mathbf{v}(t+h) = \mathbf{v}(t) + h\dot{\mathbf{v}}(t) \quad (3.11)$$

$$\dot{\mathbf{v}}(t) = \mathbf{H}(\mathbf{x}(t))^{-1}[\mathbf{u}(t) + \mathbf{u}_E(\mathbf{x}(t), \mathbf{v}(t)) - \mathbf{b}(\mathbf{x}(t), \mathbf{v}(t))] \quad (3.12)$$

where the biasing vector  $\mathbf{b}(\mathbf{x}(t), \mathbf{v}(t))$  is defined as

$$\mathbf{b}(\mathbf{x}(t), \mathbf{v}(t)) = \mathbf{C}(\mathbf{x}(t), \mathbf{v}(t))\mathbf{v}(t) + \mathbf{g}(\mathbf{x}(t)) \quad (3.13)$$

The simulation using numerical integration is described by Equations (3.8)-(3.13).

The rotating transformer  $\mathbf{T}(h\mathbf{w}_B)$  in equation (3.9) has an angle  $h|\mathbf{w}_B|$  around the  $\mathbf{w}_B$  axis. It updates the orientation matrix of the base link in response to the base link's angular velocity. It is obtained through

$$\mathbf{T}(h\mathbf{w}_B) = [(\cos(\Psi))\mathbf{I}_3 + (1 - \cos(\Psi))\mathbf{r}\mathbf{r}^T + (\sin(\Psi))[\mathbf{r}\times]] \quad (3.14)$$

where  $\Psi = h|\mathbf{w}_B|$ ,  $\mathbf{I}_3$  is  $3 \times 3$  identity matrix, and  $\mathbf{r} = \mathbf{w}_B/|\mathbf{w}_B|$ . The joint torque trajectories and the contact forces from the ground are calculated in the simulation based on the joint angles' position, velocity, and acceleration. Thus, the main aim of this framework is generating the joint torque  $\boldsymbol{\tau}$  and external force  $\mathbf{u}_E$  with using the generalized coordinates  $\mathbf{x}$ , velocities  $\mathbf{v}$ , and acceleration  $\dot{\mathbf{v}}$  which are numerically

integrated.

The Newton-Euler iterative formulation, as given in the (Luh, Walker & Paul, 1980), may be used to determine  $\mathbf{H}(x)$  and  $\mathbf{b}(x, v)$ .  $\mathbf{H}(x)$  can be computed numerically by solving inverse dynamics with  $\mathbf{x}$  equal to the present state and  $\dot{\mathbf{v}} = \mathbf{e}_j$  for  $1 \leq j \leq N + 6$ , excluding external, gravitational, centrifugal and gravitational forces.  $\mathbf{e}_j$  denotes a unit vector with all elements set to zero except the  $j^{\text{th}}$  element, set to one. Each iteration calculates the  $j^{\text{th}}$  column of the inertia matrix. Additionally, the symmetry of the inertia matrix can be used for computational purposes. By solving inverse dynamics with  $(\mathbf{x}, \mathbf{v})$  set to the current state and  $\dot{\mathbf{v}} = 0$ , neglecting external forces, the biasing vector  $\mathbf{b}(\mathbf{x}, \mathbf{v}) = \mathbf{C}(\mathbf{x}, \mathbf{v})\mathbf{v} + \mathbf{g}(\mathbf{x})$  can be calculated numerically. When given  $\mathbf{x}$ ,  $\mathbf{v}$ , and  $\dot{\mathbf{v}}$ , the left side of (3.7) can be calculated as previously mentioned by setting external forces  $f_E = 0$ . Assume the result of the left side of (3.7) is equal to  $\mathbf{u}_a$ .

$$\mathbf{u}_a(x, v, \dot{v}) = \mathbf{H}(x)\dot{v} + \mathbf{C}(x, v)v + \mathbf{g}(x) \quad (3.15)$$

which corresponds to the generalized forces generated by the inertial force, centrifugal forces, Coriolis forces, and gravity effects. The remaining issue is how to model the forces of environmental contact, i.e. how to compute the external force vector  $\mathbf{f}_E$ . The interaction forces are calculated using an adaptive penalty-based technique (Erbatur & Kawamura, 2003). The approach works by reducing the kinetic energy of the bodies in contact. After generating the external force vector  $\mathbf{f}_E$ , it is possible to obtain the generalized external force  $\mathbf{u}_E$ .

$$\mathbf{u}_e = \sum_{j \in M_A} K_j F_{Ej} = K f_E \quad (3.16)$$

where

$$M_A = \bigcup_{i=1}^N M_i \quad (3.17)$$

$K_j$  :  $(N + 6) \times 3$  matrix specifying transforms from  $j^{\text{th}}$  external force to generalized forces

$M_A$  : A set of index numbers of all active contact points

$f_E$  :  $(3M) \times 1$  vector which contains active contact forces

$K$  :  $(N + 6) \times (3M)$  matrix specifying transforms from  $f_E$  to generalized forces

$M$  : Number of time-variant active contact points.

From (3.7) and (3.16)

$$\mathbf{u}_a = \mathbf{u} + K f_E \quad (3.18)$$

$K$  can be computed by solving the inverse dynamics, with  $\mathbf{x}$  equal to the current

state,  $f_E = \mathbf{e}_j$ ,  $\dot{\mathbf{v}} = 0$ , with gravity, centrifugal, and Coriolis effects ignored. (3.18) may be rephrased as,

$$\begin{bmatrix} \mathbf{f}_a \\ \mathbf{n}_a \\ \boldsymbol{\tau}_a \end{bmatrix} = \begin{bmatrix} \mathbf{f}_B \\ \mathbf{n}_B \\ \boldsymbol{\tau} \end{bmatrix} + \begin{bmatrix} K_f \\ K_n \\ K_\tau \end{bmatrix} \mathbf{f}_E \quad (3.19)$$

where  $\mathbf{f}_B$  and  $\mathbf{n}_B$  denote the force and moment applied to the base link's origin, respectively. They are equivalent to zero for a manipulator in free fall. Then (3.19) becomes,

$$\begin{bmatrix} \mathbf{f}_a \\ \mathbf{n}_a \end{bmatrix} = \begin{bmatrix} K_f \\ N_n \end{bmatrix} \mathbf{f}_E \quad (3.20)$$

$$\boldsymbol{\tau}_a = \boldsymbol{\tau} + K_\tau \mathbf{f}_E \quad (3.21)$$

If,

$$K_{fn} = \begin{bmatrix} K_f \\ K_n \end{bmatrix} \quad (3.22)$$

has full row rank, the external force  $f_E$  solution exists in (3.20). The minimum norm solution of  $f_E$  is determined as follows:

$$f_E = K_{fn}^T (K_{fn} K_{fn}^T)^{-1} \begin{bmatrix} \mathbf{f}_a \\ \mathbf{n}_a \end{bmatrix} \quad (3.23)$$

When the matrix  $K_{fn}$  has full column rank, it is possible that no solution exist for (3.20). In this situation, the approximate solution with the minimum norm error is provided by

$$f_E = (K_{fn}^T K_{fn})^{-1} K_{fn}^T \begin{bmatrix} \mathbf{f}_a \\ \mathbf{n}_a \end{bmatrix} \quad (3.24)$$

The procedure described before determines the joint torques in the written computer simulation software. The computation loop that is followed for each step time may be listed as follows:

1. Using  $\dot{\mathbf{v}} = \mathbf{e}_j$  for  $1 \leq j \leq N+6$  to compute the inertia matrix  $\mathbf{H}(\mathbf{x})$ , solve inverse dynamics with  $\mathbf{x}$  set to the current state, neglecting centrifugal, Coriolis, gravitational, and external forces. In inverse dynamics, the disregarded forces may be adjusted to zero by setting  $\mathbf{v} = 0$ , gravitational acceleration  $g_z = 0$ , and  $f_E = 0$ . For computational reasons, this step is only performed every 100 steps.
2. Using  $\dot{\mathbf{v}} = 0$  to compute the biasing vector  $\mathbf{b}(\mathbf{x}, \mathbf{v}) = \mathbf{C}(\mathbf{x}, \mathbf{v}) + \mathbf{g}(\mathbf{x})$ , solve inverse dynamics with  $(\mathbf{x}, \mathbf{v})$  set to the current state, neglecting external forces. For computational reasons, this step is only performed every 100 steps.

3. Solve inverse dynamics equations with  $\mathbf{x}$  set to the present state,  $\mathbf{f}_E = \mathbf{e}_j$ , and  $\dot{\mathbf{v}} = 0$ , neglecting gravity, centrifugal, and Coriolis effects, to calculate the transformation matrix  $K$  numerically.
4. Calculate the generalized force  $\mathbf{u}_a$  numerically by solving inverse dynamics equations and (3.15) with setting  $(\mathbf{x}, \mathbf{v}, \dot{\mathbf{v}})$  to current state and ignoring external forces.
5. Solve (3.23) or (3.24) to generate the external force  $f_E$ . Calculate  $\mathbf{u}_E$  by (3.16).
6. Use (3.12) to calculate the generalized acceleration  $\dot{\mathbf{v}}$ .
7. By using numerical integration described in (3.8)-(3.11) and (3.14), update the generalized states  $(\mathbf{x}, \mathbf{v})$  and return to 1, for the next cycle.

The following chapter presents the reactive force control method to follow generated body reference trajectories.

#### 4. Reactive Force Control Scheme

The dynamical equation for a biped is given in (3.7). The following equation can be obtained by defining the biasing vector  $\mathbf{b}'(\mathbf{x}, \mathbf{v}) = \mathbf{C}'(\mathbf{x}, \mathbf{v}) + \mathbf{g}(\mathbf{x})$  as in (3.13) and decomposing it for body and leg dynamics. This control approach is based on the assumption that the arm joints will not be manipulated and that the arms will have no contact with the surroundings, with only the feet making touch with the ground; thus, arm dynamics are omitted.

$$\begin{bmatrix} \mathbf{H}'_{11} & \mathbf{H}'_{12} & \mathbf{H}'_{13} \\ \mathbf{H}'_{21} & \mathbf{H}'_{22} & \mathbf{H}'_{23} \\ \mathbf{H}'_{31} & \mathbf{H}'_{32} & \mathbf{H}'_{33} \end{bmatrix} \begin{pmatrix} \dot{\mathbf{v}}_B \\ \dot{\mathbf{w}}_B \\ \ddot{\boldsymbol{\theta}} \end{pmatrix} + \begin{pmatrix} \mathbf{b}'_1 \\ \mathbf{b}'_2 \\ \mathbf{b}'_3 \end{pmatrix} + \begin{pmatrix} \mathbf{u}_{E1} \\ \mathbf{u}_{E2} \\ \mathbf{u}_{E3} \end{pmatrix} = \begin{pmatrix} \mathbf{0} \\ \mathbf{0} \\ \boldsymbol{\tau} \end{pmatrix} \quad (4.1)$$

where  $\mathbf{H}'_{ij}$  for  $(i, j) \in \{1, 2, 3\}$  are sub-matrices of the  $\mathbf{H}'(\mathbf{x})$  matrix representing the robot's inertia.  $\mathbf{v}_B$  is the linear velocity of the robot's body coordinate frame center relative to a fixed world coordinate frame,  $\mathbf{w}_B$  is the angular velocity of the robot's body coordinate frame relative to a fixed world coordinate frame, and  $\boldsymbol{\theta}$  is the vector of the biped's joint displacements. The vectors  $\mathbf{b}_1$ ,  $\mathbf{b}_2$ , and  $\mathbf{b}_3$  denote the bias vector  $\mathbf{b}(\mathbf{x}, \mathbf{v})$ 's sub-vectors. The first two sub-vectors of the generalized external force vector  $\mathbf{u}_E$ ,  $\mathbf{u}_{E1}$  and  $\mathbf{u}_{E2}$ , indicate the net force and torque impacts of the robot body's response forces, respectively. The third sub-vector of the generalized external force vector,  $\mathbf{u}_{E3}$ , denotes the effect of reaction forces on the joints of the robot.  $\boldsymbol{\tau}$  is the generalized joint control vector, which for a robot with revolute joints is typically composed of joint actuation torques.  $\mathbf{H}'_{11}, \mathbf{H}'_{12}, \mathbf{H}'_{21}$ , and  $\mathbf{H}'_{22}$  are  $3 \times 3$  matrices.  $\mathbf{H}'_{13}$  is  $3 \times N$ ,  $\mathbf{H}'_{23}$  is  $3 \times N$ ,  $\mathbf{H}'_{31}$  is  $N \times 3$ ,  $\mathbf{H}'_{32}$  is  $N \times 3$ , and  $\mathbf{H}'_{33}$  is  $N \times N$ . The formulation in (4.1) demonstrates the critical nature of controlling the reactive force to control body dynamics. Because the body is not directly actuated, its dynamics are determined by the reaction force (Ayhan & Erbatur, 2004). As seen in (4.1), the body dynamics are determined by

$$\begin{bmatrix} \mathbf{H}'_{11} & \mathbf{H}'_{12} \\ \mathbf{H}'_{21} & \mathbf{H}'_{22} \end{bmatrix} \begin{pmatrix} \dot{\mathbf{v}}_B \\ \dot{\mathbf{w}}_B \end{pmatrix} + \begin{pmatrix} \mathbf{b}'_1 \\ \mathbf{b}'_2 \end{pmatrix} + \begin{bmatrix} \mathbf{H}'_{13} \\ \mathbf{H}'_{23} \end{bmatrix} \ddot{\boldsymbol{\theta}} + \begin{pmatrix} \mathbf{u}_{E1} \\ \mathbf{u}_{E2} \end{pmatrix} = \begin{pmatrix} \mathbf{0} \\ \mathbf{0} \end{pmatrix} \quad (4.2)$$

This, in a compact version, may be stated as

$$\tilde{\mathbf{H}}\dot{\mathbf{r}} + \tilde{\mathbf{b}} + \boldsymbol{\tau}_{dis} = \boldsymbol{\tau}_E \quad (4.3)$$

where

$$\mathbf{r} = \begin{pmatrix} \dot{\mathbf{v}}_B \\ \dot{\mathbf{w}}_B \end{pmatrix}, \quad \tilde{\mathbf{b}} = \begin{pmatrix} \mathbf{b}'_1 \\ \mathbf{b}'_2 \end{pmatrix}, \quad \boldsymbol{\tau}_{dis} = \begin{bmatrix} \mathbf{H}'_{13} \\ \mathbf{H}'_{23} \end{bmatrix} \ddot{\boldsymbol{\theta}}, \quad \boldsymbol{\tau}_E = \begin{pmatrix} \mathbf{u}_{E1} \\ \mathbf{u}_{E2} \end{pmatrix} \quad (4.4)$$

Leg dynamics are ignored, and reaction forces are used as a control input. Given the body trajectories, inverse dynamics generates reference reaction forces. The tracking errors for the body can be defined as

$$\begin{pmatrix} \mathbf{e}_{posbody} \\ \mathbf{e}_{rotbody} \end{pmatrix} = \begin{pmatrix} \mathbf{p}_{Bref} - \mathbf{p}_B \\ 0.5 \left( \mathbf{n}_{body} \times \mathbf{n}_{bodyref} + \mathbf{s}_{body} \times \mathbf{s}_{bodyref} + \mathbf{a}_{body} \times \mathbf{a}_{bodyref} \right) \end{pmatrix} \quad (4.5)$$

$$\begin{pmatrix} \dot{\mathbf{e}}_{posbody} \\ \dot{\mathbf{e}}_{rotbody} \end{pmatrix} = \begin{pmatrix} \mathbf{v}_{Bref} - \mathbf{v}_B \\ \mathbf{w}_{Bref} - \mathbf{w}_B \end{pmatrix}$$

where  $\mathbf{e}_{posbody}$  refers to the body's Cartesian position error and  $\mathbf{e}_{rotbody}$  refers to the body's orientation error. The column vectors of the body rotation matrix are  $\mathbf{n}_{body}$ ,  $\mathbf{s}_{body}$  and  $\mathbf{a}_{body}$ .

$$\mathbf{R}_{body} = \begin{bmatrix} \mathbf{n}_{body} & \mathbf{s}_{body} & \mathbf{a}_{body} \end{bmatrix} \quad (4.6)$$

A equivalent rotation matrix for the body's reference orientation is also defined.

$$\mathbf{R}_{bodyref} = \begin{bmatrix} \mathbf{n}_{bodyref} & \mathbf{s}_{bodyref} & \mathbf{a}_{bodyref} \end{bmatrix} \quad (4.7)$$

In actuality, the expression for computing the orientation error for the body coordinate frame,  $0.5 \left( \mathbf{n}_{body} \times \mathbf{n}_{bodyref} + \mathbf{s}_{body} \times \mathbf{s}_{bodyref} + \mathbf{a}_{body} \times \mathbf{a}_{bodyref} \right)$ , is an approximation. The cross-products used to calculate the orientation errors can be analyzed and shown to approximate the orientation errors for small angles (Figure 4.1).

$$\begin{aligned} \mathbf{n}_{body} \times \mathbf{n}_{bodyref} &\approx \sin \theta_s \mathbf{s}_{body} + \sin \theta_a \mathbf{a}_{body} \approx \theta_s \mathbf{s}_{body} + \theta_a \mathbf{a}_{body} \\ \mathbf{s}_{body} \times \mathbf{s}_{bodyref} &\approx \sin \theta_a \mathbf{a}_{body} + \sin \theta_n \mathbf{n}_{body} \approx \theta_a \mathbf{a}_{body} + \theta_n \mathbf{n}_{body} \\ \mathbf{a}_{body} \times \mathbf{a}_{bodyref} &\approx \sin \theta_s \mathbf{s}_{body} + \sin \theta_n \mathbf{n}_{body} \approx \theta_s \mathbf{s}_{body} + \theta_n \mathbf{n}_{body} \end{aligned} \quad (4.8)$$

Therefore,

$$\begin{aligned} 0.5 \left( \mathbf{n}_{body} \times \mathbf{n}_{bodyref} + \mathbf{s}_{body} \times \mathbf{s}_{bodyref} + \mathbf{a}_{body} \times \mathbf{a}_{bodyref} \right) \\ \approx \theta_n \mathbf{n}_{bodyref} + \theta_s \mathbf{s}_{bodyref} + \theta_a \mathbf{a}_{bodyref} \end{aligned} \quad (4.9)$$

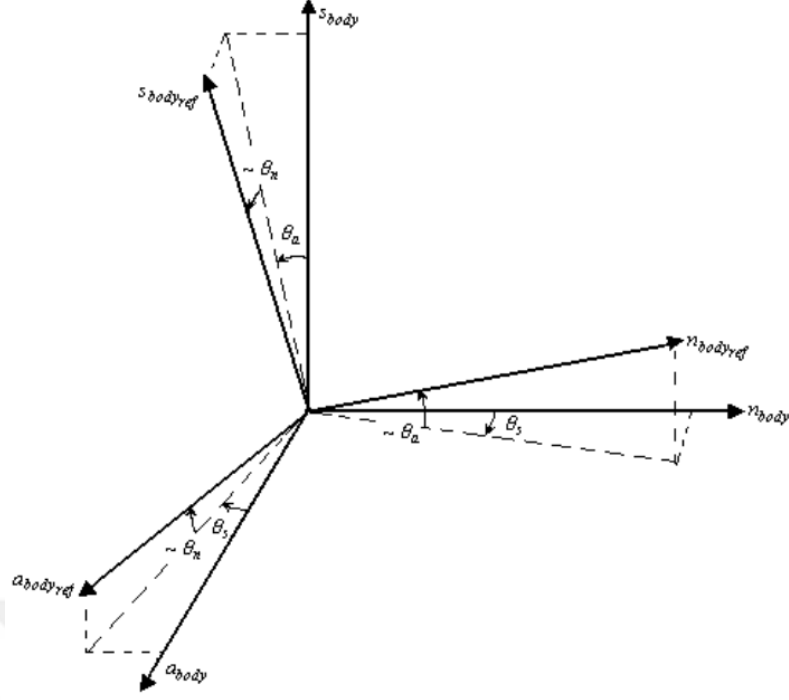


Figure 4.1 For small angles, definition of orientation error

After specifying the tracking errors for the body, the non-linear plant is transformed to second-order dynamics using the following control rule.

$$\mathbf{v} = \mathbf{K}_p \begin{pmatrix} e_{pos_{body}} \\ e_{rot_{body}} \end{pmatrix} + \mathbf{K}_d \begin{pmatrix} \dot{e}_{pos_{body}} \\ \dot{e}_{rot_{body}} \end{pmatrix} + \begin{pmatrix} \dot{\mathbf{v}}_{B_{ref}} \\ \dot{\boldsymbol{\omega}}_{B_{ref}} \end{pmatrix} \quad (4.10)$$

$$\begin{pmatrix} \mathbf{u}_{E1_{ref}} \\ \mathbf{u}_{E2_{ref}} \end{pmatrix} = \begin{bmatrix} \mathbf{H}'_{11} & \mathbf{H}'_{12} \\ \mathbf{H}'_{21} & \mathbf{H}'_{22} \end{bmatrix} \mathbf{v} + \begin{pmatrix} \mathbf{b}'_1 \\ \mathbf{b}'_2 \end{pmatrix} \quad (4.11)$$

where  $\mathbf{K}_p$  and  $\mathbf{K}_d$  are control designer-defined parameters specifying the desired dynamics. Referring to (3.16), references for ground interaction forces and reference body forces and torques can be related by the equation.

$$\begin{pmatrix} \mathbf{u}_{E1_{ref}} \\ \mathbf{u}_{E2_{ref}} \end{pmatrix} = \mathbf{K}' \mathbf{f}_{E_{ref}} \quad (4.12)$$

where  $\mathbf{K}'$  is the  $6 \times (3M)$  sub-matrix of  $\mathbf{K} = \begin{bmatrix} \mathbf{K}' \\ \mathbf{K}'' \end{bmatrix}$  and related to the ground interaction forces on the foot corners to the reactive force and torque applied on the robot body. The bottom half of the matrix  $\mathbf{K}$  is referred to as  $\mathbf{K}''$ , and it is the matrix that describes the relationship between contact forces and reaction forces at

joints and it is  $N \times (3M)$ .  $\mathbf{K}'$  is in the form of

$$\mathbf{K}' = \begin{bmatrix} \mathbf{I}_3 & \mathbf{I}_3 & \mathbf{I}_3 & \mathbf{I}_3 \\ (\mathbf{d} + \mathbf{c}_1) \times & (\mathbf{d} + \mathbf{c}_2) \times & (\mathbf{d} + \mathbf{c}_3) \times & (\mathbf{d} + \mathbf{c}_4) \times \end{bmatrix} \quad (4.13)$$

where

$\mathbf{c}_j$  :  $3 \times 1$  position vector of  $j^{th}$  contact point with respect to the foot center as shown in Figure 4.2.

$\mathbf{d}$  :  $3 \times 1$  position vector of foot center with respect to the base link coordinate frame.

$\mathbf{I}_3$  :  $(3M) \times 3$  identity matrix.

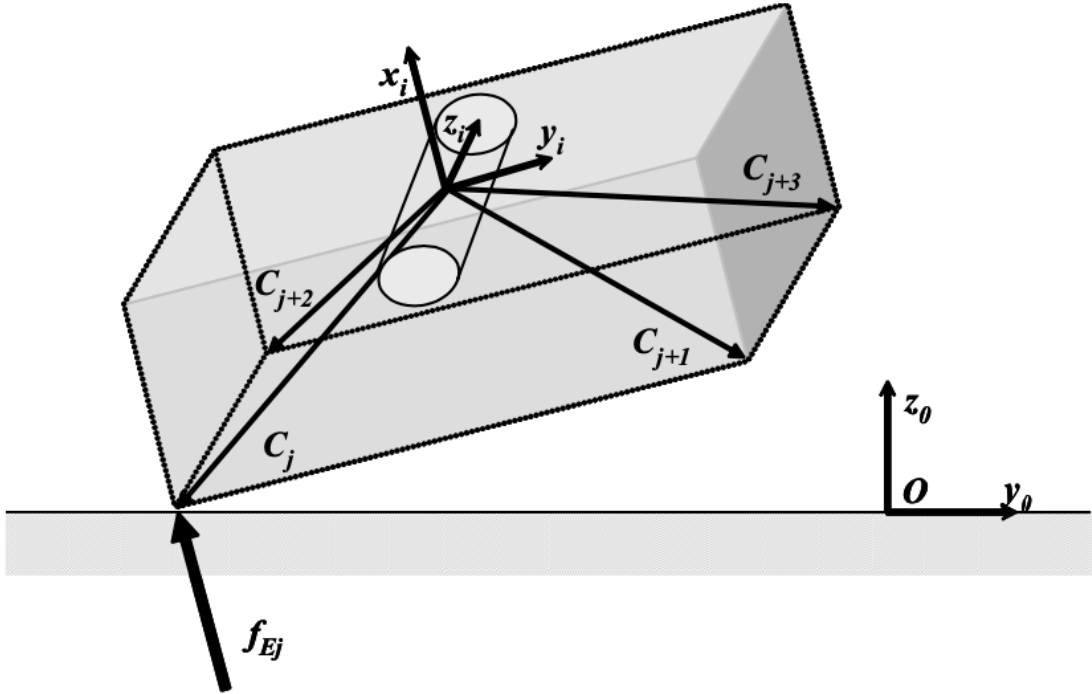


Figure 4.2 Contact Points of the foot

Therefore

$$\begin{pmatrix} \mathbf{u}_{E1ref} \\ \mathbf{u}_{E2ref} \end{pmatrix} = \mathbf{K}' \mathbf{f}_{Eref} = \begin{pmatrix} \sum_{j \in M_A} \mathbf{f}_{Ej} \\ \mathbf{d} \times \sum_{j \in M_A} \mathbf{f}_{Ej} + \sum_{j \in M_A} \mathbf{c}_j \times \mathbf{f}_{Ej} \end{pmatrix} \quad (4.14)$$

(4.12) is solved to obtain the forces at the foot references. However, (4.12) presents an under-determined set of equations. Furthermore, not every system solution is physically feasible because to the non-attractive nature of the contact, and the no-slip criterion that must be satisfied for stability. Let  $\mathbf{f}_{E_i} = [\mathbf{f}_{E_{ix}} \ \mathbf{f}_{E_{iy}} \ \mathbf{f}_{E_{iz}}]$ ,  $i \in$

$\{1, 2, \dots, 8\}$ . Based on the non-attractive nature of the contact

$$\mathbf{f}_{E_{iz}} \geq 0, \quad \forall i \in \{1, 2, \dots, 8\} \quad (4.15)$$

The constraint for no-slip is

$$-\mu \leq \frac{\sqrt{\mathbf{f}_{E_{ix}}^2 + \mathbf{f}_{E_{iy}}^2}}{\mathbf{f}_{E_{iz}}} \leq \mu, \quad \forall i \in \{1, 2, \dots, 8\} \quad (4.16)$$

In (4.16), the inequality is a nonlinear constraint. Optimization with constraints is used to compute a set of ground contact forces for biped locomotion. Approximating the nonlinear constraint in (4.16) by

$$\begin{aligned} -\frac{\sqrt{2}}{2}\mu &\leq \frac{\mathbf{f}_{E_{ix}}}{\mathbf{f}_{E_{iz}}} \leq \frac{\sqrt{2}}{2}\mu \\ -\frac{\sqrt{2}}{2}\mu &\leq \frac{\mathbf{f}_{E_{iy}}}{\mathbf{f}_{E_{iz}}} \leq \frac{\sqrt{2}}{2}\mu, \quad \forall i \in \{1, 2, \dots, 8\} \end{aligned} \quad (4.17)$$

(4.17), although more conservative than (4.16), is a collection of linear restrictions, which simplifies the problem. (4.15) and (4.17) can be compressed into the form shown below.

$$A\mathbf{f}_{E_{ref}} \leq 0 \quad (4.18)$$

where  $A$  is a  $24 \times 24$  matrix derived from these constraint inequalities. The issue becomes getting  $\mathbf{f}_E$  with this formulation,

$$\begin{aligned} \min_{\mathbf{f}_{E_{ref}}} & \left\| \mathbf{K}' \mathbf{f}_{E_{ref}} - \begin{pmatrix} \mathbf{u}_{E_{1ref}} \\ \mathbf{u}_{E_{2ref}} \end{pmatrix} \right\|^2 \\ \text{s.t.} & \quad A\mathbf{f}_{E_{ref}} \leq 0 \end{aligned} \quad (4.19)$$

Sequential quadratic programming is used to solve this linear restricted least-squares issue. This thesis does not go into depth on the optimization process. However, (Rardin, 2017) has details on this optimization strategy. The optimization algorithm's solution is directly converted to joint torques as follows:

$$\mathbf{u}_{E_{3ref}} = \mathbf{K}'' \mathbf{f}_{E_{ref}} \quad (4.20)$$

There are infinitely many solutions to the optimization scheme, but they all correspond to a single foot center force, torque, and joint reference torques. With the reference joint torque application, only one of the solutions set will be realized. The optimization scheme picks one solution arbitrarily, irrelevant of whether they obey

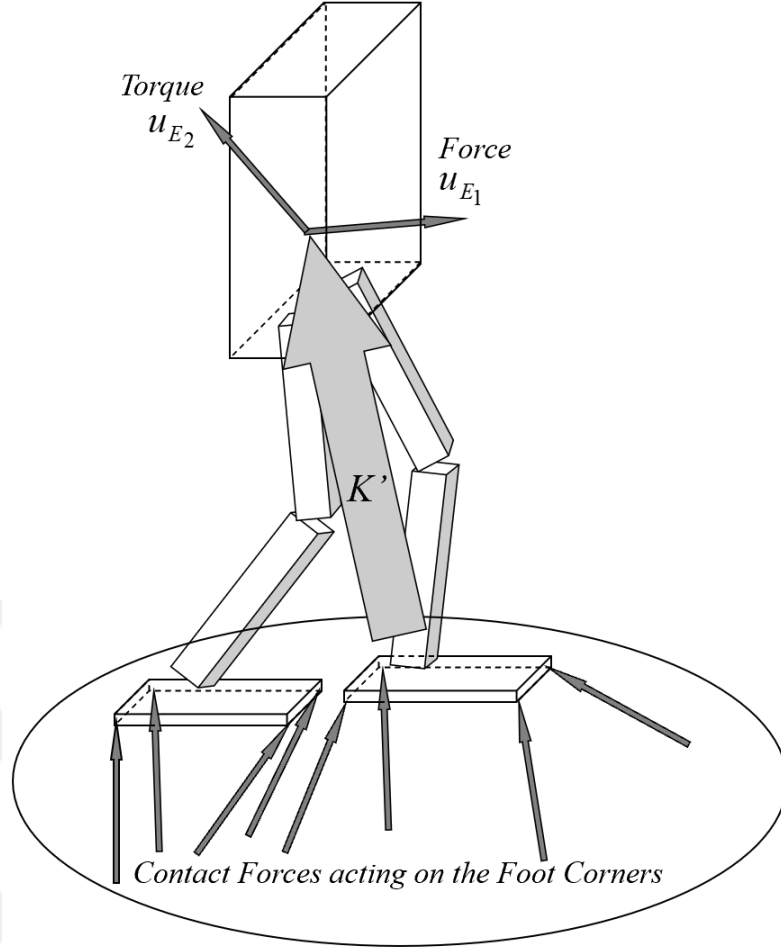


Figure 4.3 The matrix  $\mathbf{K}'$  establishes a relationship between the reactive force and torque given to the robot's body and the ground contact forces at the robot's foot corners.

the compatibility relations. Whatever solution is picked, the optimization ends in the same joint torque reference. After applying this joint torque, the arising contact force, which probably is different from the reference contact force, is an element of the feasible set of solutions for the optimization scheme. Thus, the objective is not to track the reference contact forces, since this is impossible, but to guarantee that the contact forces perform their assigned functions by providing specific information.

After obtaining the reference reaction forces on joints  $\boldsymbol{\tau}_{ref} = \mathbf{u}_{E3ref} + \mathbf{b}'_3$  will track reference reaction forces at steady-state, considering the leg dynamics:

$$\mathbf{H}'_{33}\ddot{\boldsymbol{\theta}} + \begin{bmatrix} \mathbf{H}'_{31} & \mathbf{H}'_{32} \end{bmatrix} \begin{pmatrix} \dot{\mathbf{v}}_B \\ \dot{\mathbf{w}}_B \end{pmatrix} + \mathbf{b}'_3 + \mathbf{u}_{E3} = \boldsymbol{\tau} \quad (4.21)$$

This chapter described how the legs are used to follow a given body trajectory reference via reactive force control. The next chapter proposes using this method to keep balancing while applying pushing force with both arms.

## 5. Biped Balance With Reactive Force Control Scheme

Chapter 4 summarized how body posture is controlled by setting the response forces on the supporting leg or legs. While the reactive force control scheme is the primary control system used while walking, it can also be employed to maintain balance when manipulating an object or applying force on an object. In this thesis, the biped robot pushes a wall with both arms during the double support phase and preserves its balance. The robot's motion is divided into two steps. The first step involves moving the arms to contact the wall; the second involves applying the necessary force.

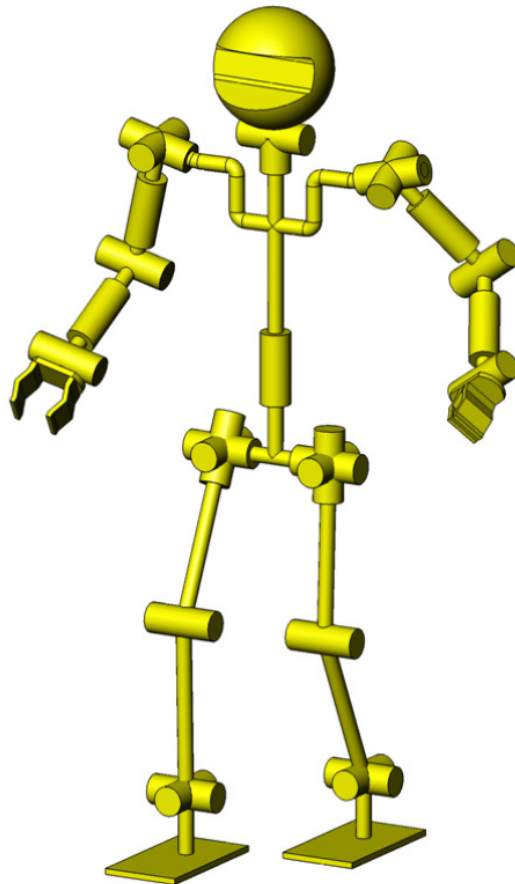


Figure 5.1 The kinematic arrangement of SURALP

Upper Leg Length	280mm
Lower leg length	270mm
Ankle center to foot sole distance	124mm
Foot dimensions	240mm x 150mm
Upper arm length	219mm
Lower arm length	255mm
Robot weight	114 kg

Table 5.1 Dimensions and weight data of SURALP

The dynamical equations for a bipedal robot is defined as in (3.7). If the bias vector is defined as  $\mathbf{b}(\mathbf{x}, \mathbf{v}) = \mathbf{C}(\mathbf{x}, \mathbf{v}) + \mathbf{g}(\mathbf{x})$  same as in (3.13), the following equation may be formed by the biasing vector as in reference and decomposing it for body, leg, and arm dynamics. The kinematic structure of the robot SURALP robot can be seen in Figure 5.1.

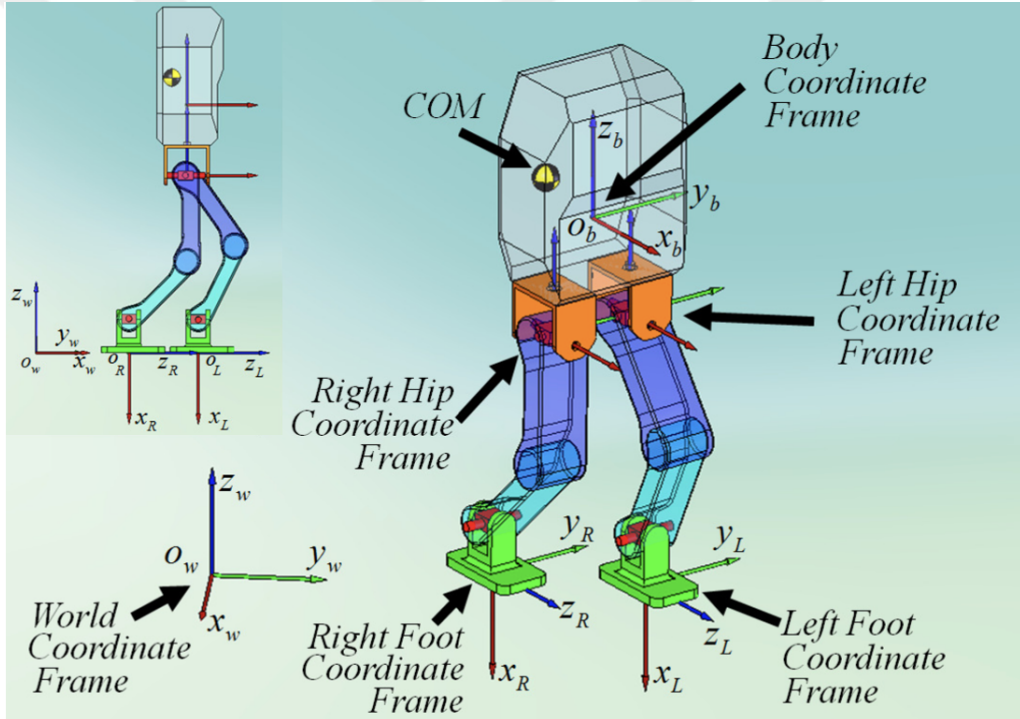


Figure 5.2 SURALP's coordinate systems.  $o_w$  and  $o_b$  denote the world's origins and body coordinate frames, respectively.

$$\begin{bmatrix} \mathbf{H}_{11} & \mathbf{H}_{12} & \mathbf{H}_{13} \\ \mathbf{H}_{21} & \mathbf{H}_{22} & \mathbf{H}_{23} \\ \mathbf{H}_{31} & \mathbf{H}_{32} & \mathbf{H}_{33} \end{bmatrix} \begin{pmatrix} \dot{\mathbf{v}}_B \\ \dot{\boldsymbol{\omega}}_B \\ \ddot{\boldsymbol{\theta}} \end{pmatrix} + \begin{pmatrix} \mathbf{b}_1 \\ \mathbf{b}_2 \\ \mathbf{b}_3 \end{pmatrix} + \begin{pmatrix} \mathbf{u}_{E1} \\ \mathbf{u}_{E2} \\ \mathbf{u}_{E3} \end{pmatrix} = \begin{pmatrix} \mathbf{0} \\ \mathbf{0} \\ \boldsymbol{\tau} \end{pmatrix} \quad (5.1)$$

where  $\mathbf{H}_{ij}$  for  $(i,j) \in \{1,2,3\}$  are sub-matrices of the  $\mathbf{H}(\mathbf{x})$  matrix representing the robot's inertia.  $\mathbf{v}_B$  is the linear velocity of the robot's body coordinate frame center relative to a fixed world coordinate frame,  $\boldsymbol{\omega}_B$  is the angular velocity of the

robot's body coordinate frame relative to a fixed world coordinate frame, and  $\boldsymbol{\theta}$  is the vector of the biped's joint displacements. The vectors  $\mathbf{b}_1$ ,  $\mathbf{b}_2$ , and  $\mathbf{b}_3$  denote the bias vector  $\mathbf{b}(\mathbf{x}, \mathbf{v})$ 's sub-vectors. The first two sub-vectors of the generalized external force vector  $\mathbf{u}_E$ ,  $\mathbf{u}_{E_1}$  and  $\mathbf{u}_{E_2}$ , indicate the net force and torque effects on the robot body, respectively. The third sub-vector of the generalized external force vector,  $\mathbf{u}_{E_3}$ , denotes the effect of reaction forces on the joints of the robot.  $\boldsymbol{\tau}$  is the generalized joint control vector, which for a robot with revolute joints is typically composed of joint actuation torques.  $\mathbf{H}_{11}, \mathbf{H}_{12}, \mathbf{H}_{21}$ , and  $\mathbf{H}_{22}$  are  $3 \times 3$  matrices.  $\mathbf{H}_{13}$  is  $3 \times N$ ,  $\mathbf{H}_{23}$  is  $3 \times N$ ,  $\mathbf{H}_{31}$  is  $N \times 3$ ,  $\mathbf{H}_{32}$  is  $N \times 3$ , and  $\mathbf{H}_{33}$  is  $N \times N$ . To be noted here is that these matrices are constructed with considering dynamics of body, legs, and arms, unlike the reaction force control scheme in Chapter 4 where only body and legs are included.

As seen in (5.1), the body dynamics are determined by

$$\begin{bmatrix} \mathbf{H}_{11} & \mathbf{H}_{12} \\ \mathbf{H}_{21} & \mathbf{H}_{22} \end{bmatrix} \begin{pmatrix} \dot{\mathbf{v}}_B \\ \dot{\mathbf{w}}_B \end{pmatrix} + \begin{pmatrix} \mathbf{b}_1 \\ \mathbf{b}_2 \end{pmatrix} + \begin{bmatrix} \mathbf{H}_{13} \\ \mathbf{H}_{23} \end{bmatrix} \ddot{\boldsymbol{\theta}} + \begin{pmatrix} \mathbf{u}_{E_1} \\ \mathbf{u}_{E_2} \end{pmatrix} = \begin{pmatrix} \mathbf{0} \\ \mathbf{0} \end{pmatrix} \quad (5.2)$$

## 5.1 Reaching the Wall

To make contact with the wall, the trunk-based position reference trajectory of the arm's endpoint is generated. Because the arm's trajectory is defined as a linear line, the reference trajectory in the y and z axes always remain constant. Reference in x axis is defined as

$$x_{endpoint}^{ref}(t) = 0.05t \quad (5.3)$$

where  $t$  is time. The y coordinate of the right hand at -0.375 m and the left hand at symmetrically at 0.375 m with respect to the body coordinate frame at the pelvis of the robot. The z-directional reference is 0.29 m with respect to the same frame. This corresponds to a height of 0.9 m in world frame coordinate. The initial robot posture and the posture at the wall touching instant are shown in Figure 5.3.

The desired joint positions  $\mathbf{q}_{arm_d}$  are generated using inverse kinematics based on the position and orientation references of the arm's endpoint.

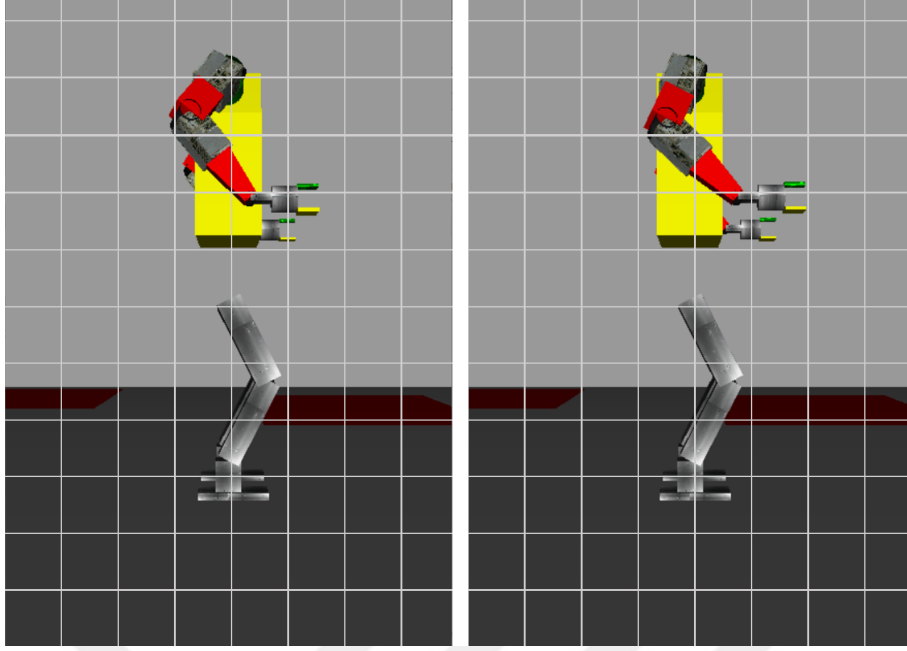


Figure 5.3 Snapshots from the OpenGL based animation window. Robot initial configuration (left) and the configuration at the wall contact instant with hands moved forward (right). Initial conditions of the hands are 0.235 m in the world coordinate frame. The wall is not shown in animation. It is placed at 0.3 m parallel to the world frame y-z plane. Two snapshots above described the robot motion before the wall contact.

The hand frame desired orientation with respect to the body frame is given by,

$$A_{bref}^h = \begin{bmatrix} 1 & 0 & 0 \\ 0 & 0 & 1 \\ 0 & -1 & 0 \end{bmatrix} \quad (5.4)$$

which corresponds to the fingers. Forward orientation of the hands shown in Figure 5.3.

Independent joint position PID controllers are used to track arm tip position references derived by inverse kinematics.  $\tau_{arm}^{right}, \tau_{arm}^{left}$  are obtained as in (5.5). Gains for PID controllers ( $K_p^{arm}, K_i^{arm}, K_d^{arm}$ ) are obtained by trial and error.

$$\tau_{arm} = K_p^{arm} (\mathbf{q}_{arm_d} - \mathbf{q}_{arm}) + K_d^{arm} (\dot{\mathbf{q}}_{arm_d} - \dot{\mathbf{q}}_{arm}) + K_i^{arm} \int (\mathbf{q}_{arm_d} - \mathbf{q}_{arm}) dt \quad (5.5)$$

The arm links track the desired positions, and as an outcome of this manipulation, naturally, the robot's body shifts. Therefore, the robot should balance this manipulation's additional force/torque effect on the body to keep it at its desired position.

The reactive force control scheme is implemented to generate ground reaction forces. For this purpose, reference body reaction force are generated based on body dynamics (5.2). The tracking errors for the body can be defined as in (4.5). The inverse dynamics method is used for generating body reference reaction forces  $\mathbf{u}_{E_{1ref}}^{legs}$  and  $\mathbf{u}_{E_{2ref}}^{legs}$  as in following.

$$\mathbf{v} = \mathbf{K}_p \begin{pmatrix} \mathbf{e}_{posbody} \\ \mathbf{e}_{rotbody} \end{pmatrix} + \mathbf{K}_d \begin{pmatrix} \dot{\mathbf{e}}_{posbody} \\ \dot{\mathbf{e}}_{rotbody} \end{pmatrix} + \begin{pmatrix} \dot{\mathbf{v}}_{B_{ref}} \\ \dot{\boldsymbol{\omega}}_{B_{ref}} \end{pmatrix} \quad (5.6)$$

$$\begin{pmatrix} \mathbf{u}_{E_{1ref}} \\ \mathbf{u}_{E_{2ref}} \end{pmatrix} = \begin{bmatrix} \mathbf{H}_{11} & \mathbf{H}_{12} \\ \mathbf{H}_{21} & \mathbf{H}_{22} \end{bmatrix} \mathbf{v} + \begin{pmatrix} \mathbf{b}_1 \\ \mathbf{b}_2 \end{pmatrix} \quad (5.7)$$

where  $\mathbf{K}_p$  and  $\mathbf{K}_d$  are control designer-defined parameters specifying the desired dynamics.

The ground interaction reference forces on the foot corners are calculated for reactive force and torque applied on the robot body. Since not every system solution is physically feasible, the optimization technique (4.19) is used to obtain ground interaction forces. Since both arms are in position control and are not in touch with the environment, the same  $\mathbf{K}'$  matrix as Chapter 4 can be employed in optimization calculations. The robot can preserve its current position and orientation by optimizing ground reaction forces when the two feet are in touch with the ground, and slipping conditions are met. Since (5.6) is providing a feedback effect on the body position and orientation, optimized ground reaction forces can compensate for the additional force/torque effect on the body during the arm motion. The solution of the optimization process is directly transformed to joint torques for legs  $\mathbf{u}_{E_{3ref}}^{legs}$  as in (4.20). the same  $\mathbf{K}''$  matrix as Chapter 4 can be employed in for joint torque calculation.

The following expression can be used for the generalized joint torque vector  $\mathbf{u}_{E_{3ref}}$ .

$$\mathbf{u}_{E_{3ref}} = \begin{pmatrix} \mathbf{u}_{E_{3ref}legs} \\ \boldsymbol{\tau}_{arm}^{right} \\ \boldsymbol{\tau}_{arm}^{left} \end{pmatrix} \quad (5.8)$$

The arms are controlled independently of the base and both legs, while the base and both legs are controlled by the reactive force controller.

## 5.2 Maintaining Balance While Pushing

### 5.2.1 Generate Body Reference Reaction Forces

After executing the first part successfully, the control mode is switched from maintaining balance while arm position control without hand contact to maintaining balance while pushing the wall with desired forces.

As one of the stability criteria, ZMP denotes a point on the ground where the tangential components of the moment created by the ground reaction force/moment are zero. While ZMP is inside the convex hull of the foot-supporting area, the robot will maintain its balance. The ZMP will be determined by the contact forces applied by the hands, and it should be generalized to define stability during pushing manipulation (Harada, Kajita, Saito, Morisawa, Kanehiro, Fujiwara, Kaneko & Hirukawa, 2005). If the hand contact force is small enough, the robot will maintain its ZMP within the supporting area. However, the ZMP will shift outside the supporting area when the applied force is higher.

To maintain ZMP constrained inside the convex hull of the foot-supporting region, the robot can adjust its posture, therefore shifting the CoM, or it can balance pushing force with ground contact forces. In this thesis, balancing via compensation of the pushing force with ground force is considered. The hand contact force references are begin at zero and increase linearly to the desired level. Different cases have been implemented to observe the effectiveness of the method. The below, these two approaches for generating body reference reaction forces have been described.

#### 5.2.1.1 First Case

The body dynamics (5.2) is actuated with external forces. The tracking errors for the body can be defined as in (4.5). The body reference reaction forces can be generated by inverse dynamics approach as follows.

$$\mathbf{v} = \mathbf{K}_p \begin{pmatrix} e_{pos_{body}} \\ e_{rot_{body}} \end{pmatrix} + \mathbf{K}_d \begin{pmatrix} \dot{e}_{pos_{body}} \\ \dot{e}_{rot_{body}} \end{pmatrix} + \begin{pmatrix} \dot{\mathbf{v}}_{B_{ref}} \\ \dot{\mathbf{w}}_{B_{ref}} \end{pmatrix} \quad (5.9)$$

$$\begin{pmatrix} \mathbf{u}_{E_{1ref}} \\ \mathbf{u}_{E_{2ref}} \end{pmatrix} = \begin{bmatrix} \mathbf{H}_{11} & \mathbf{H}_{12} \\ \mathbf{H}_{21} & \mathbf{H}_{22} \end{bmatrix} \mathbf{v} + \begin{pmatrix} \mathbf{b}_1 \\ \mathbf{b}_2 \end{pmatrix} \quad (5.10)$$

where  $\mathbf{K}_p$  and  $\mathbf{K}_d$  are control designer-defined parameters specifying the desired dynamics. Reference body reaction force are generated based on the conservation of ideal position and orientation of the base.

### 5.2.1.2 Second Case

The definitions of body dynamics and the tracking errors for the body are the same as Subsection 5.2.1.1. In the proposed new method, the x-axis of reference body reaction force is enhanced to match the influence of total hand reaction forces on the body. The inverse dynamics method can be used to create the body reference response forces as below.

$$\mathbf{v} = \mathbf{K}_p \begin{pmatrix} e_{pos_{body}} \\ e_{rot_{body}} \end{pmatrix} + \mathbf{K}_d \begin{pmatrix} \dot{e}_{pos_{body}} \\ \dot{e}_{rot_{body}} \end{pmatrix} \quad (5.11)$$

$$\begin{pmatrix} \mathbf{u}_{E_{1ref}} \\ \mathbf{u}_{E_{2ref}} \end{pmatrix} = \mathbf{S}_{cbody} \left( \begin{bmatrix} \mathbf{H}_{11} & \mathbf{H}_{12} \\ \mathbf{H}_{21} & \mathbf{H}_{22} \end{bmatrix} \mathbf{v} + \begin{pmatrix} \mathbf{b}_1 \\ \mathbf{b}_2 \end{pmatrix} \right) + \mathbf{S}_{body} \begin{bmatrix} 2 * K'_{arm_x} f_{E_{refarms_x}}(t) \\ \mathbf{0}_{5 \times 1} \end{bmatrix} \quad (5.12)$$

where  $K'_{arm_x}$  is the element of  $\mathbf{K}'$  matrix that link the reactive force on the robot's body to interaction force.  $\mathbf{K}'$  is different from the one described in Chapter 4 since the ground and hand reaction forces are included in contact model.  $K'_{arm_x}$  is the element that link the reactive force on the robot's body in the x-direction to the desired hand contact forces in x direction  $f_{E_{refarms_x}}$ . Reference hand contact forces begin at zero and linearly increase to the desired force in two seconds for both arms after the arm endpoints contact with the wall.  $\mathbf{S}_{body}$  and  $\mathbf{S}_{cbody}$  are selection matrices composed of zeros and ones. For  $\mathbf{S}_{cbody}$ , the x-component of the multiplication result vector will be zero, while the other components will remain unchanged. Additionally, for the  $\mathbf{S}_{body}$ , the x-component of the multiplication result will be the same, while the other components will be zero.

In body reaction force, the x-axis is enhanced to match the influence of total hand reaction forces on the body. Thus, reference body reaction forces are generated not just based on conservation of fixed body posture but also balance the effect of pushing force on the body.

### 5.2.2 Generate Leg Joint Torques Via Body Reference Reaction Force

The following equation can be used to relate ground contact forces and reference body forces and torques.

$$\begin{pmatrix} \mathbf{u}_{E_{1ref}} \\ \mathbf{u}_{E_{2ref}} \end{pmatrix} = \mathbf{K}'_{leg} \mathbf{f}_{E_{ref}legs} \quad (5.13)$$

where  $\mathbf{K}'_{leg}$  is the sub-matrix of  $\mathbf{K}'$  and link the reactive force on the robot's body to the reference ground contact force  $\mathbf{f}_{E_{ref}legs}$ .

$$\begin{aligned} \min_{\mathbf{f}_{E_{ref}legs}} & \quad \left\| \mathbf{K}'_{leg} \mathbf{f}_{E_{ref}legs} - \begin{pmatrix} \mathbf{u}_{E_{1ref}} \\ \mathbf{u}_{E_{2ref}} \end{pmatrix} \right\|^2 \\ \text{s.t.} & \quad A \mathbf{f}_{E_{ref}legs} \leq 0 \end{aligned} \quad (5.14)$$

The optimization result is directly converted to joint torques for legs  $\mathbf{u}_{E_{3ref}}^{legs}$ , as,

$$\mathbf{u}_{E_{3ref}legs} = \mathbf{K}''_{leg} \mathbf{f}_{E_{ref}legs} \quad (5.15)$$

where  $\mathbf{K}''_{leg}$  is the sub-matrix of  $\mathbf{K}''$  and link ground contact forces to reaction forces on leg joints.

### 5.2.3 Arm Hybrid Control and Generation of Generalized Joint Torques

Unlike the reaching the wall task, arm manipulation is accomplished using a hybrid control method. First, a PD cartesian position control is applied to conserve the initial contact point's y-z position with the wall in order to generate the desired arm endpoint force.  $\mathbf{f}_{arm}^{right}$  and  $\mathbf{f}_{arm}^{left}$  can be calculated as following.

$$\mathbf{f}_{arm} = \mathbf{K}'_p \begin{pmatrix} \mathbf{e}_{posarm} \\ \mathbf{e}_{rotarm} \end{pmatrix} + \mathbf{K}'_d \begin{pmatrix} \dot{\mathbf{e}}_{posarm} \\ \dot{\mathbf{e}}_{rotarm} \end{pmatrix} \quad (5.16)$$

Since the obtained force only keeps the arm in touch with the wall at its initial contact point, the x-axis of the  $\mathbf{f}_{E_{ref}arms}$  is different from the desired applied force  $\mathbf{f}_{E_{ref}armsx}$ . Thus, the desired force term overrides the x-directional desired force term in (5.16).

$$\mathbf{f}_{arm} = \begin{pmatrix} f_{E_{ref}armsx} \\ f_{army} \\ f_{armz} \end{pmatrix} \quad (5.17)$$

The  $x$ -component of reference hand contact force is set to the desired pushing force.

$$\begin{aligned} \boldsymbol{\tau}_{arm}^{right} &= \mathbf{K}_{arm}^{right} \mathbf{f}_{arm}^{right} \\ \boldsymbol{\tau}_{arm}^{left} &= \mathbf{K}_{arm}^{left} \mathbf{f}_{arm}^{left} \end{aligned} \quad (5.18)$$

where  $\mathbf{K}_{arm}^{right}$  and  $\mathbf{K}_{arm}^{left}$  is the sub-matrix of  $\mathbf{K}''_{arm}$  and link hand contact forces to reaction forces on arm joints. As a result, the generalized joint torque vector  $\mathbf{u}_{E_{3ref}}$  is formed as

$$\mathbf{u}_{E_{3ref}} = \begin{pmatrix} \mathbf{u}_{E_{3ref}legs} \\ \boldsymbol{\tau}_{arm}^{right} \\ \boldsymbol{\tau}_{arm}^{left} \end{pmatrix} \quad (5.19)$$

### 5.3 A Simple technique for Comparison Purposes

In this section, a purely position controller system is discussed. The body and leg are defined in the world coordinate frame and the hand configurations are defined in the body coordinate frame. The world frame reference for the body corresponds to the standing posture in Figure 5.4 and the hands move to a target of 0.1 m deep inside the wall with a constant velocity. All joint position references are obtained via inverse kinematics. Leg joint positions references are obtained with inverse kinematics computations using the foot position and orientation references with respect to the robot body frame. Similarly hand position and orientation references with respect to the body frame provide inputs for hand-to-body inverse kinematics algorithms. All inverse kinematics methods are analytic and rely on geometric considerations. They are not presented in this thesis work in detail. Joint position references are tracked with PID controllers. This technique is a simple one when compared with the two reaction force based approaches discussed before in this chapter. However it is a case demonstrating the robot-wall interaction in the absence of force based control algorithms.

## 5.4 Block Diagrams

The three cases, namely the simple technique of Section 5.3, the first case of reactive force control in Subsection 5.2.1.1 and the second case in Subsection 5.2.1.2 are summarized in the block diagrams below.

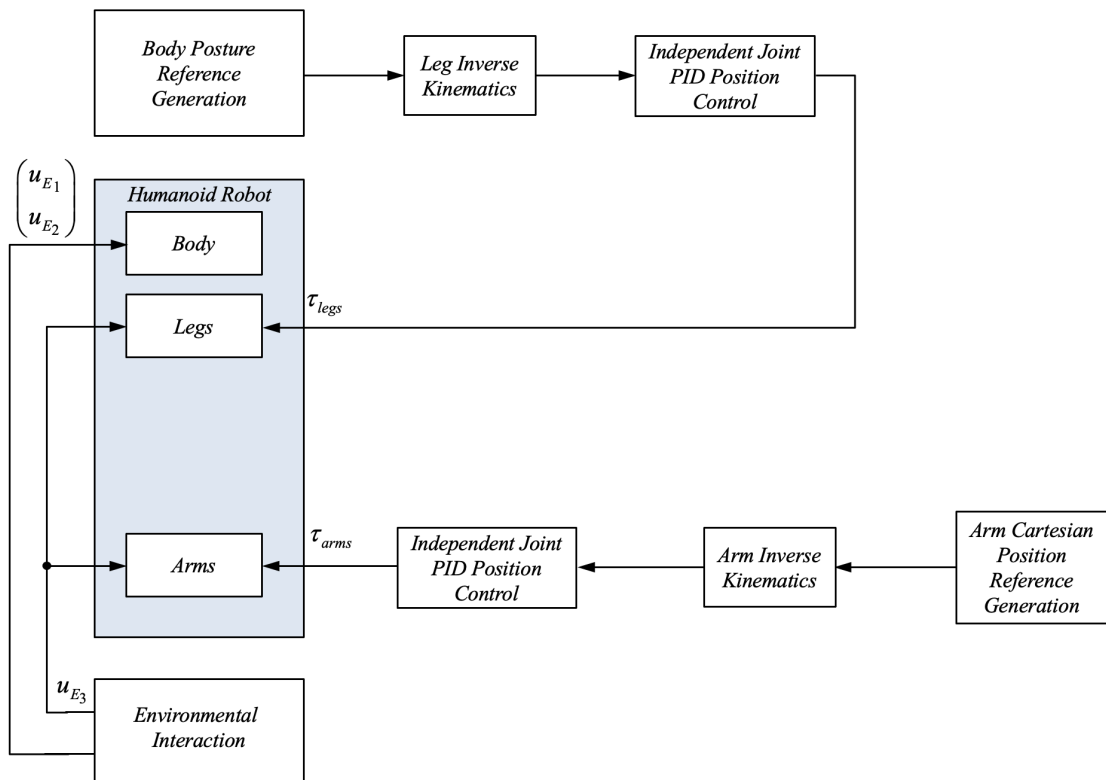


Figure 5.4 The block diagram of the simple independent joint position control based technique

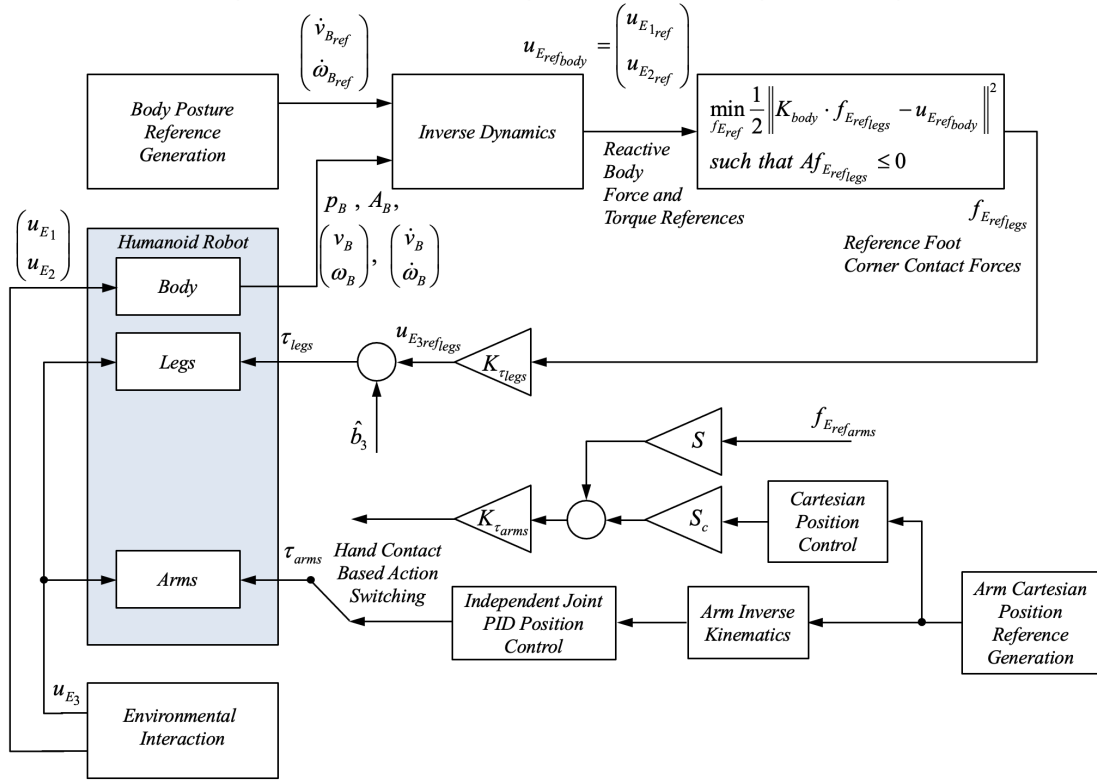


Figure 5.5 Reactive Force Control Case 1. Body is aimed to be kept at its original posture via reactive force control. Hybrid control is implemented for the arms.

$S$  and  $S_c$  are selection matrices to choose position control in tangential directions and feed-forward force control in the direction towards the wall.

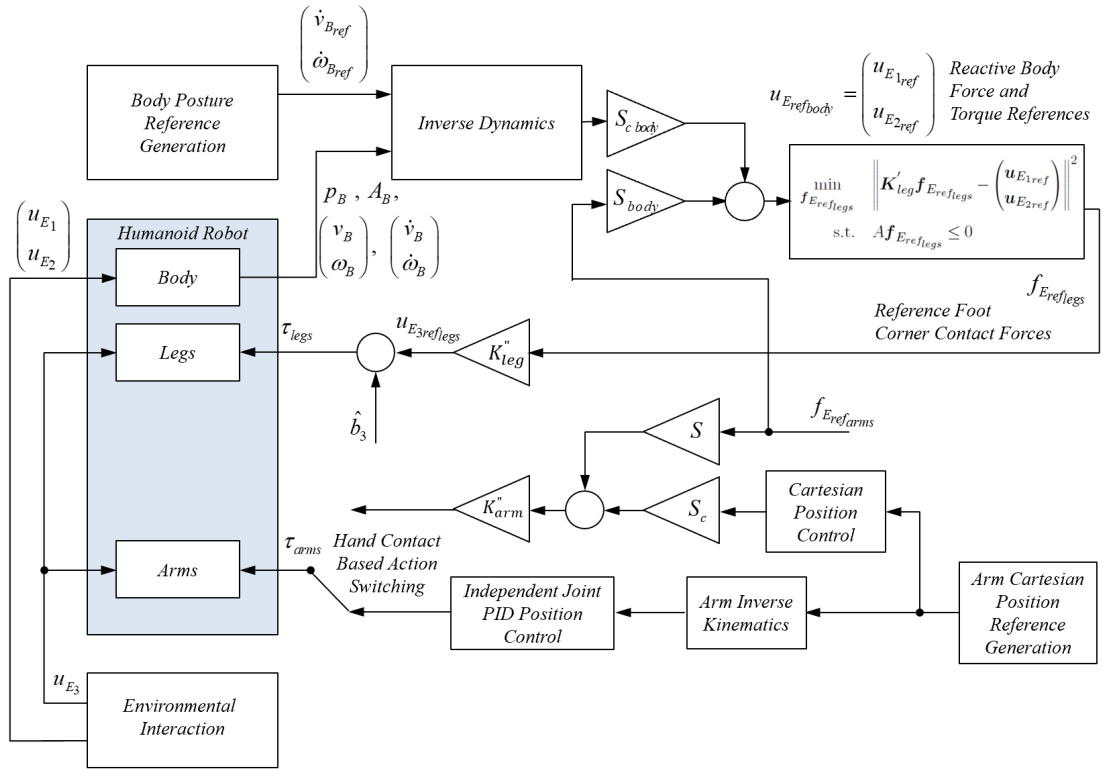


Figure 5.6 Reactive Force Control Case 2. Body receives a feed-forward wall contact force when hand touched the wall.

$S_{body}$  and  $S_{cbody}$  are selection matrices to choose feed-forward force control in the wall direction and position control in other directions.

Reactive Force Control Case 1 and its improved version Reactive Force Control Case 2 constitute our contribution in this thesis. Techniques above are simulated and simulation results are presented in the next Chapter with comparisons.

## 6. Simulation Results

This chapter discusses the simulation results for the proposed control method using the 30 DOF biped model SURALP.

Simulink simulations with a sampling duration of 0.5 milliseconds and Euler integration are used. The simulation technique is similar to (Ayhan, 2004), explained in Chapter 3. The reactive force control technique presented in Chapter 5.

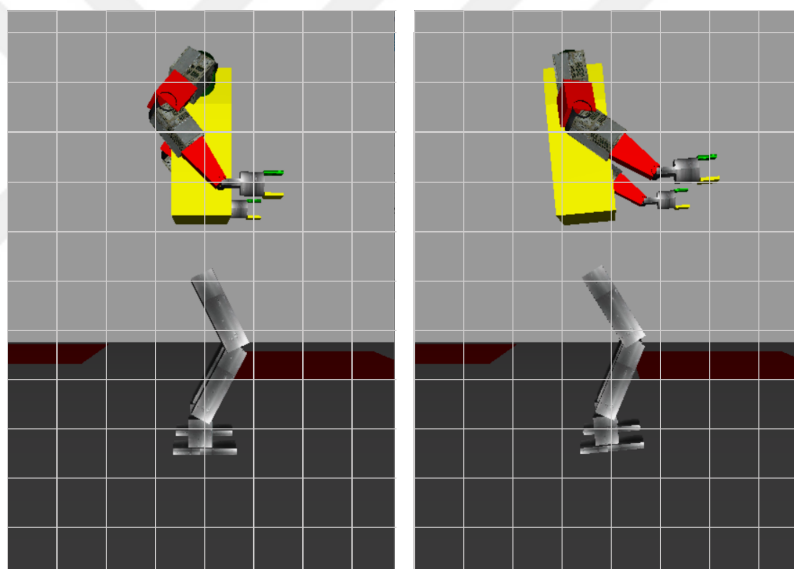


Figure 6.1 Snapshots from the OpenGL based animation window. Robot initial configuration (left) and the configuration when hands moved forward to 0.4 m in the body coordinate frame(right). Hand keep the contact with wall and push the body away from it. The wall is not shown in animation. It is placed at 0.3 m parallel to the world frame y-z plane. The initial configuration is picture is the same as in Figure 5.3 and is given here in order to compare initial and final configurations side by side. Note that in the right hand side picture, the arms are extended to 0.4 m in the x-direction where as the right hand side picture of Figure 5.3 shows hands stopped at 0.3 m, at the wall.

As mentioned in Chapter 5, simulations are carried out with a basic position control based approach illustrated in Figure 5.4. Animation snapshots with this method are shown in Figure 6.1. The picture on the left shows the initial configuration and the

one on the right shows the steady state. The robot body is pushed towards back and is supported by the heels and the hands. The robot keeps its configuration in the body frame. However its orientation is dramatically affected when seen in the world frame. This example motivates more advanced techniques of control when the robot interacts with the environment over hand contact.

## 6.1 Robot Arm Manipulation Via Position Control

As described in Section 5.1, to achieve contact with the wall, the trunk-based position reference trajectory of the endpoint of the arm is derived as

$$\begin{pmatrix} x_{endpoint}^{ref} \\ y_{endpoint}^{ref} \\ z_{endpoint}^{ref} \end{pmatrix} = \begin{pmatrix} 0.05t \\ \mp 0.375 \\ 0.29 \end{pmatrix} \quad (6.1)$$

where,  $y_{endpoint}^{ref}$  is negative for right hand and positive for left hand and  $t$  is time.

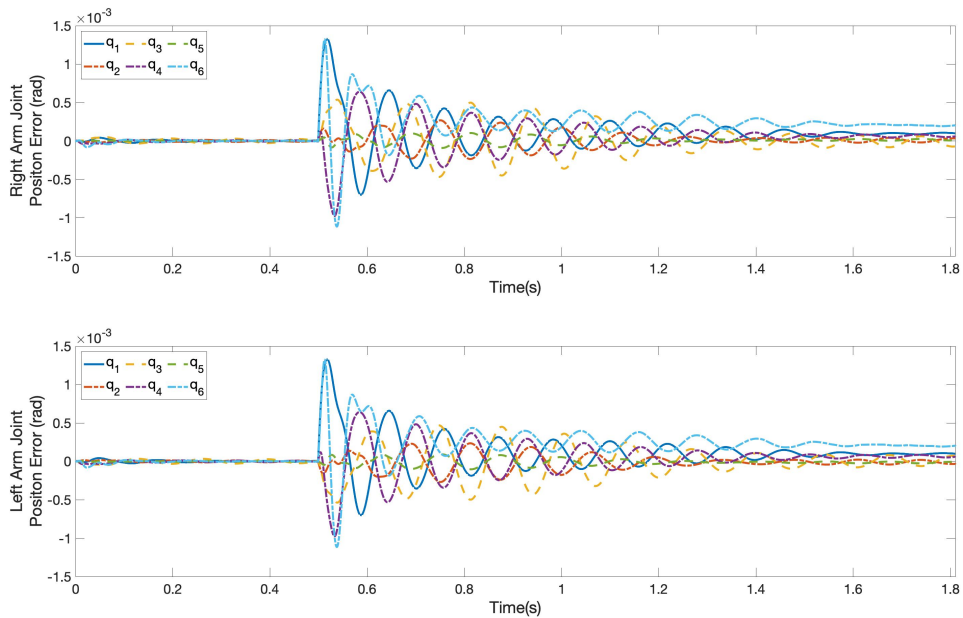


Figure 6.2 Arm joint position error during reaching the wall

The PID gains that describes the arm dynamics are chosen as

$$\begin{aligned}
 \mathbf{K}_p^{arm} &= \text{diag}[6000, 20000, 20000, 30000, 30000, 9000] \\
 \mathbf{K}_d^{arm} &= \text{diag}[1, 1, 1, 1, 1, 1] \\
 \mathbf{K}_i^{arm} &= \text{diag}[40, 40, 40, 40, 40, 40]
 \end{aligned} \tag{6.2}$$

by trial and error. Figure 6.2 shows arm joint position errors during the motion towards the wall with selected PID gain matrices. Various linear reference trajectories with fixed and varying hand orientations are used in tuning the gains. Joint position references are obtained with inverse kinematics and joint angular position errors less than 0.01 rad. in the transient sought. Classical control design and tuning techniques directly applicable to linear time invariant systems are not employed here because of the highly nonlinear and coupled plant equations.

## 6.2 Generation of Ground Reaction Forces

This section presents the case study of two different approaches to generating ground reaction forces based on reference body reaction forces. As noted in Subsection 5.2.1.1, the first case assumes the forces acting on the base only keep the robot in the fixed body posture with inverse dynamic calculation (5.9)-(5.10). Following that, Figure 6.3 and Figure 6.5 illustrate the robot's ground reaction forces on contact points and center of pressure of the robot (CoP), respectively. The desired applied pushing force to the wall is defined as 90 N for each arm in these graphs.

Contact points are defined as the corners of each foot; consequently, there are a total of eight possible contact points. As seen from the Figure 6.3, the ground reaction forces on the contact points at the heel increase as the applied pushing force increases. The peak value at 1.8 seconds corresponds to the time when the initial contact is made. Due to the speed of the robot arm at the time of contact, the wall contact force reaches 100 N, but then rapidly decreases and follows the desired force profile.

The base dynamics are directly actuated, but the ground reaction forces determine it. The control algorithm for Case 1 aims to preserve the robot's fixed posture with optimization for ground reaction forces without considering hand reaction force. The base has an acceleration and its position shifting towards heels as seen in Figure 6.4, and in order to preserve the body posture, the ground reaction forces at the heels

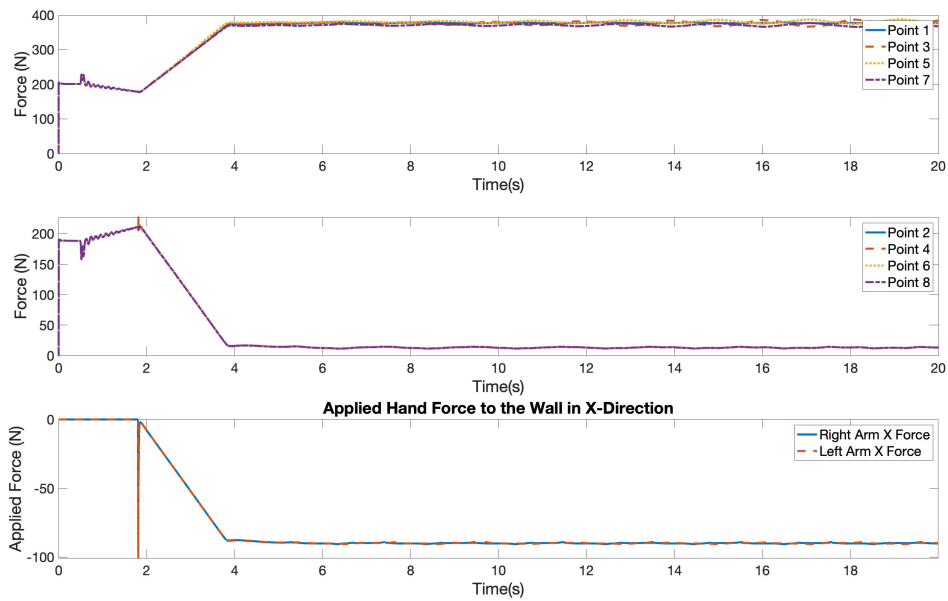


Figure 6.3 Ground reaction forces at contact points in z-axis for Case 1

are much higher than the ones on the toes. The difference between contact forces at heel and toes are approximately 360 N.

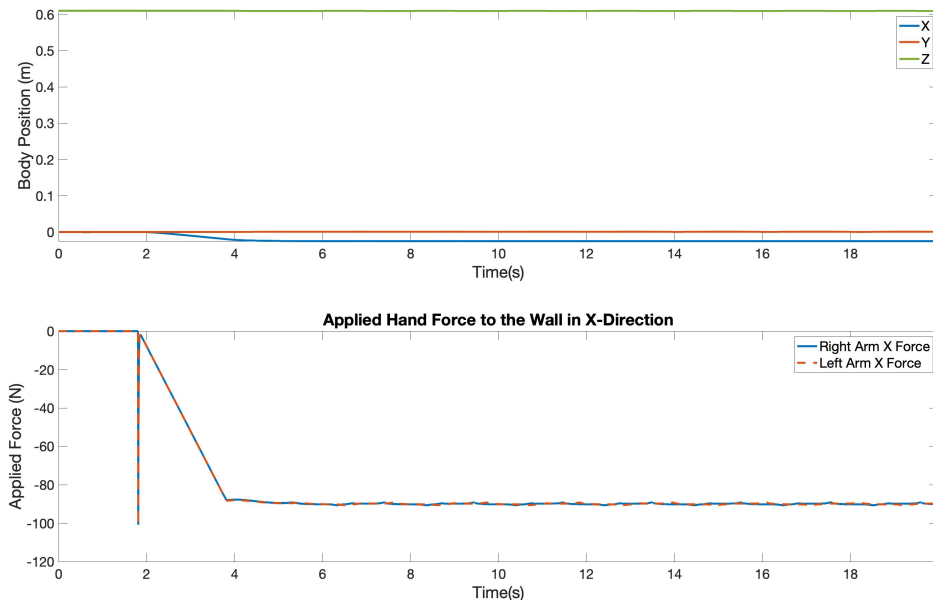


Figure 6.4 Position of the base for Case 1

The presence of hand reaction forces and the difference between contact forces at heel and toes lead to a the center of pressure shift to the heels that is to the boundary of the foot support polygon as seen in Figure 6.5. The distance of the CoP to the

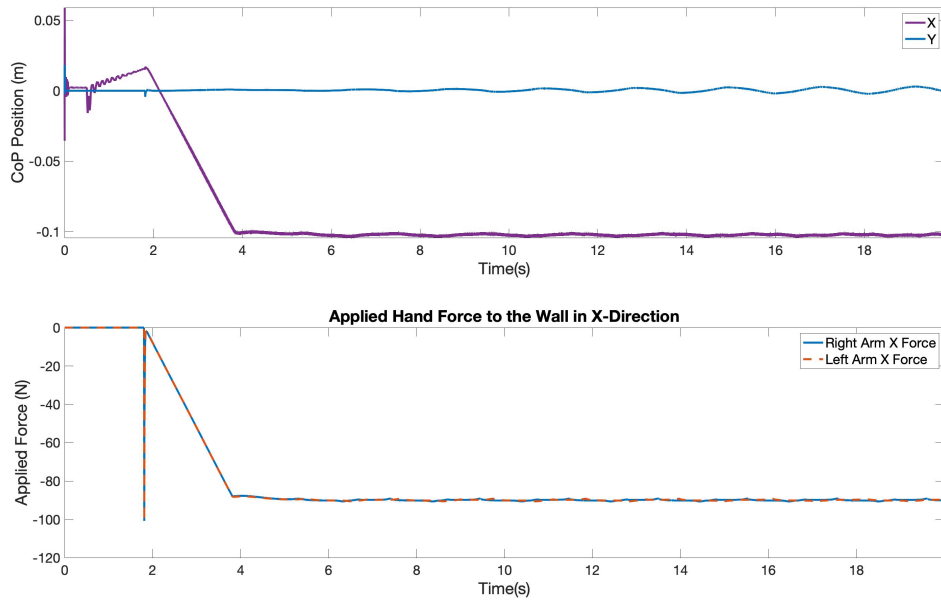


Figure 6.5 Position of the center of pressure for Case 1

support polygon is one of the stability criteria for the balance of the stance.

For stability, CoP should be constrained inside the convex hull of the foot-supporting region, and as seen from the Figure 6.5, CoP is at the border of the defined region. In the simulation studies, the target force (the reference force ramp saturation value) is increased in a series of tests.

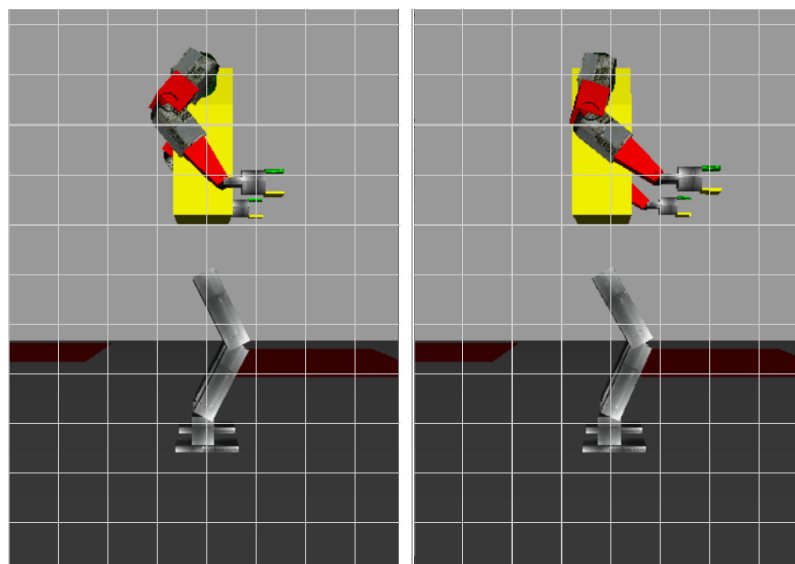


Figure 6.6 Robot initial posture (left), robot applies 94 N per hand (right) at the wall successfully. The initial posture is not different from the ones in Figures 5.3 and 6.1. It is shown here for a side by side comparison with the final configuration. Case 1 of reactive control: Body posture kept essentially at the initial condition in contrast to the basic position control case shown in Figure 6.1.

The biped could keep the contact on eight foot corners up to a value of 94 N target force per hand. With higher target values the robot loses its balance. The initial and final robot posture are shown Figure 6.6 with snapshots from the animation window.

In the second case, reference body reaction forces and reference applied pushing forces are added in order to keep the robot in the fixed body posture calculated in inverse dynamics while supporting the hand reaction forces. Thus, ground reaction forces are more appropriately distributed for the pushing force, unlike in the first case. First, to compare the mentioned two cases, the result of the experiment where the pushing force for both arms is equal to 90 N is presented. Then, the upper limit target force of the second case will be searched via simulations.

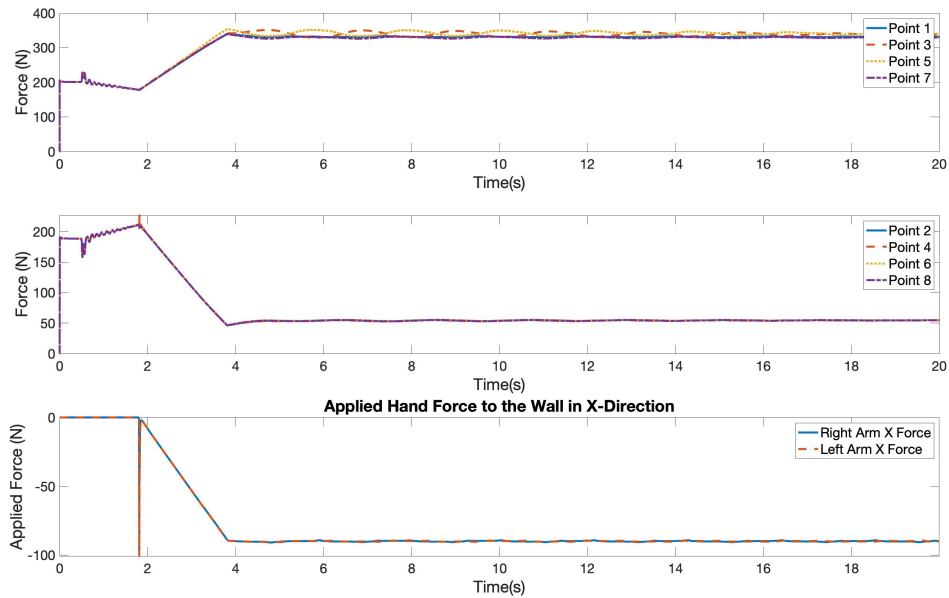


Figure 6.7 Ground reaction forces at contact points in z-axis for Case 2, applied force is 90 N

As seen from the Figure 6.7, in the proposed method, same as Case 1, ground reaction forces at heels are higher than the ones on the toes. As can be observed, the main difference between the two approaches is that the forces at the heel and toe are distributed more evenly, and the imbalance between them is reduced to about 280 N.

The control method for Case 2, results in a significantly lower body acceleration than the first case and even a positive acceleration, as seen in the Figure 6.8. Positive acceleration is critical because the biped robot is expected to lean forward while applying force on the wall. Although controlling the robot's pitching angle for forward-leaning is not part of this thesis, this finding is worth noting.

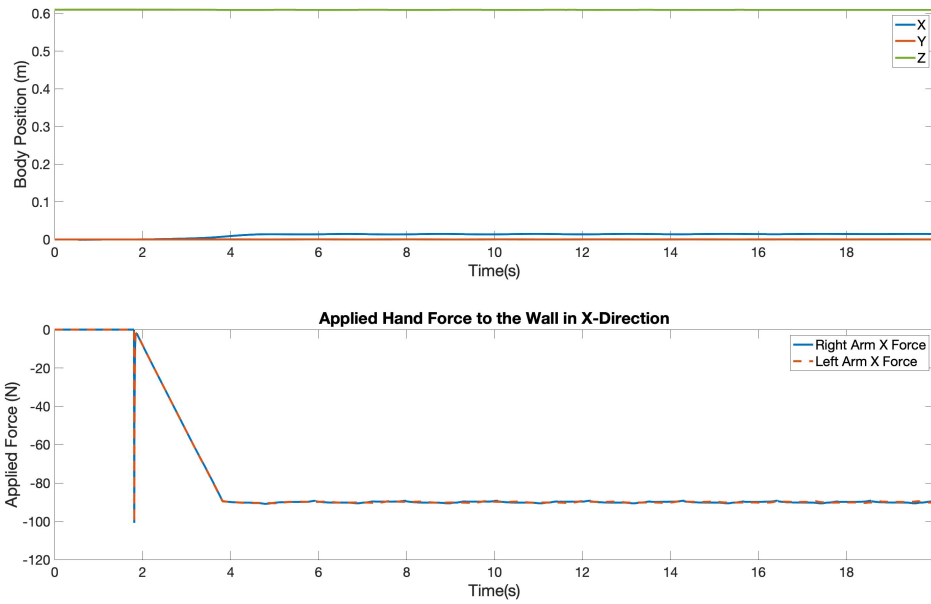


Figure 6.8 Position of the base for case 2, applied force is 90 N

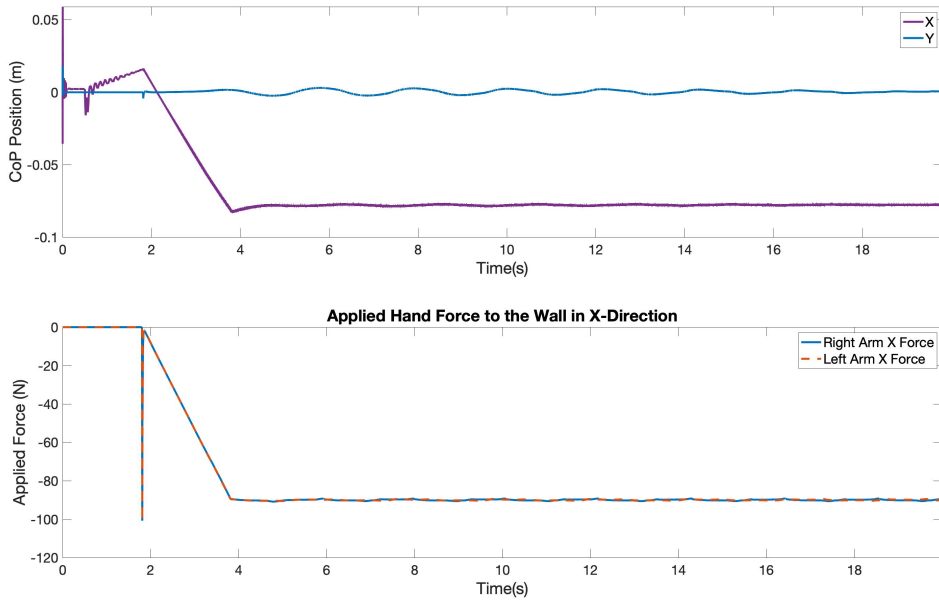


Figure 6.9 Position of the center of pressure for Case 2, applied force is 90 N

Due to the more uniform distribution of ground response forces and their capability to balance hand reaction forces, the CoP is placed closer to the base in Case 2 than in Case 1, as seen in the Figure 6.9. In Case 1, the maximum pushing force for each hand is 94 N; hence, CoP is the boundary of the support convex hull at this value. However, it is evident that in Case 2, there is greater flexibility in increasing

the pushing force applied by the hands. Simulations indicate that the maximum pushing force for each hand advanced to 117 N.

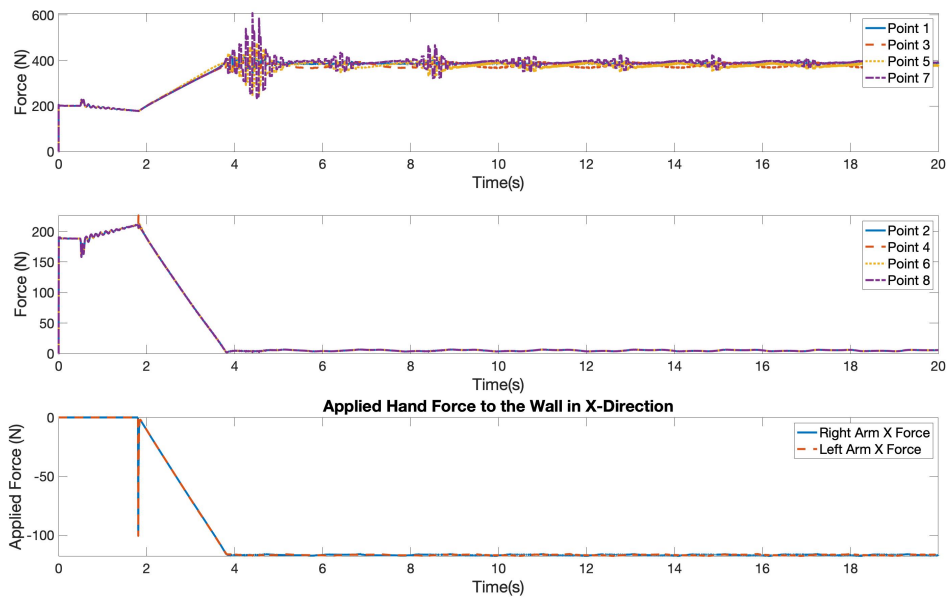


Figure 6.10 Ground reaction forces at contact points in z-axis for Case 2, applied force is 117 N

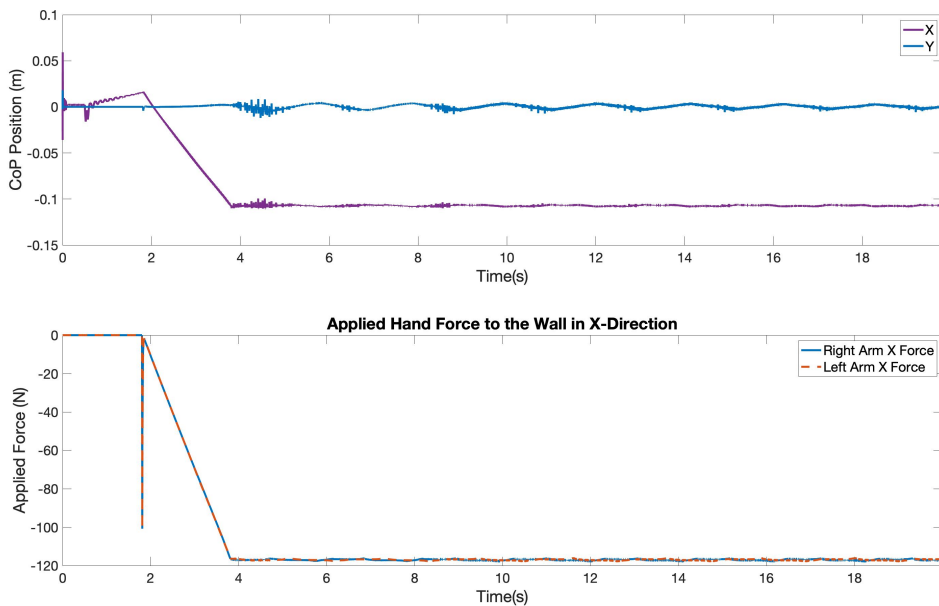


Figure 6.11 Position of the center of pressure for Case 2, applied force is 117 N

As seen in Figure 6.10, the ground response forces at the toes are in the order of 5 N and at the heels are at about 390N with the 117 N pushing force for each arm.

This is the maximum value for not falling backward. This outcome implies that the reaction forces at the robot's heels are responsible for balancing the robot for hand reaction forces and preserving its posture. High oscillations at the heels are due to the lack of reaction forces at the toes and the large hand reaction force levels. The initial and steady state pictures of the robot arm shown in Figure 6.12 with a 117 N force value per hand contact.

As expected, the CoP is at the border of the convex support hull in the x-axis at the limit as seen as in Figure 6.11. Even though the base position is inside the convex support hull and satisfies the static balance criteria, after the upper limit of pushing force, CoP reaches the boundary, and the robot falls backward.

Case 1 allows for a pushing force of 94 N with both arms, whereas Case 2 achieves a pushing force of to 117 N. Thus, foot force optimization with push support resulted in a 24.468 percent increase in the applied force.

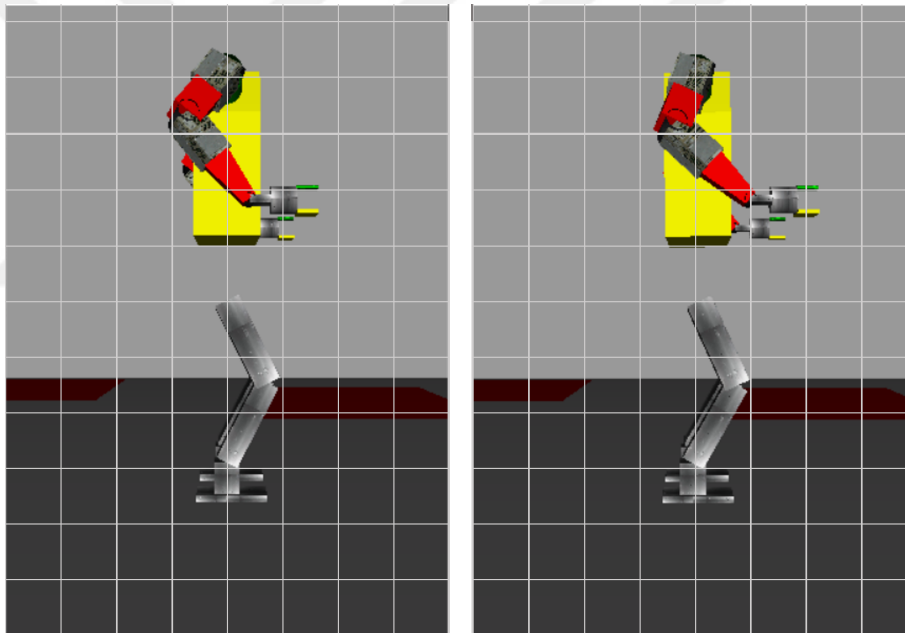


Figure 6.12 Snapshots from the OpenGL based animation window. Robot initial configuration (left) and the configuration in the steady state (right). The left hand side picture is not different from the initial posture pictures in Figures 5.3, 6.1 and 6.6. It is shown here for a side by side comparison with the final configuration on the right. Case 2 of reactive control. The wall is not shown in animation. It is placed at 0.3 m parallel to the world frame y-z plane. A comparison of the right hand side picture in this figure with the right hand side picture with in Figure 6.6 (Case 1 of Reactive Control) shows that the robot body moves slightly closer to the wall with Case 2. The wall contact force reference is used in a feed-forward fashion for the body control force reference and this reference created the leaning-on-the-wall effect shown in the picture.

### 6.3 On Robot Arm Control via Hybrid Control

In both Case 1 and Case 2 the arms are under hybrid position force control. This section presents details about this technique with Case 2 data. As described in Subsection 5.2.3, hybrid control aims to preserve the location of the contact point even while applying the pushing desired force to do the wall. The PD gains utilized in arm cartesian position control are as follows.

$$\begin{aligned} \mathbf{K}_p^{\prime arm} &= \text{diag}[36, 100, 100] \\ \mathbf{K}_d^{\prime arm} &= \text{diag}[12, 20, 20] \end{aligned} \quad (6.3)$$

After calculating the desired arm endpoint force for the contact position conservation is obtained, the x-axis force is overridden by the desired pushing force. In the discussion which follows, the desired pushing force for each hand is 117 N.

Figure 6.13 shows the arm endpoint position for the y-z axes. With the cartesian position control, the contact point is closely tracked and the desired pushing force in the x-direction is also achieved.

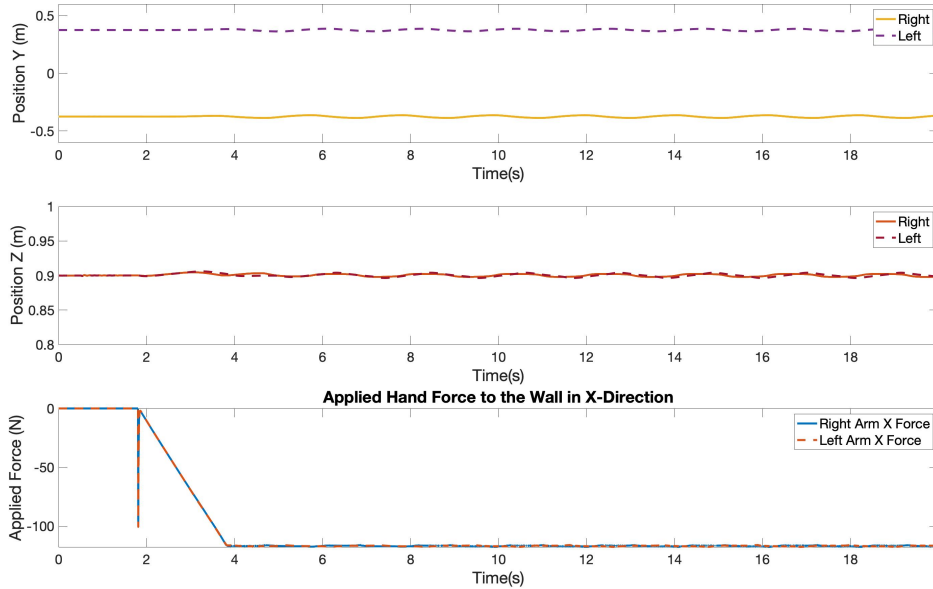


Figure 6.13 Arm endpoint positions for Case 2, applied force is 117 N

## 7. Conclusion

This thesis presents two humanoid robot control approaches on exerting force on a wall through hands without changing foot locations. The methods are based on computing suitable foot-ground interaction forces and generating them through leg joint torques. Achieving a large force application capacity on the wall without losing robot balance is an important target in this study. Our first approach, Case 1, aims at keeping the body at a fixed posture, while in our final design, namely Case 2, the reference pushing force is added to the body reaction forces. With Case 2, the addition of pushing force effect on the body posture control increased the pushing force capacity by approximately 25%.

The two methods mentioned above address the hand force application on fixed foot locations through ground contact force management, and in this respect they are different from the studies reported in the literature. The addition of hand manipulation forces and torques on the body reactive forces is promising for other full-body humanoid tasks as well.

A future study direction can be to explore walking trajectory generation with simultaneous manipulation tasks carried out by hands. Improving pushing force capacity by changing foot positions is another approach that can be studied. Expanding full-body control applications to other manipulation tasks can be investigated as well. Examples of other manipulation tasks could be opening a door, pulling an object, or carrying a heavy load.

## BIBLIOGRAPHY

- Ayhan, O. (2004). *Biped locomotion control via hybrid position control and gravity compensation modes* /. Thesis-Sabancı University.
- Ayhan, O. & Erbatur, K. (2004). Biped Robot Walk Control Via Gravity Compensation Techniques. In *30th Annual Conference of IEEE Industrial Electronics Society, 2004. IECON 2004*, volume 1, (pp. 621–626)., Busan, South Korea. IEEE.
- Cheng, G., Hyon, S.-h., Morimoto, J., Ude, A., Colvin, G., Scroggin, W., & Jacobsen, S. C. (2006). CB: A Humanoid Research Platform for Exploring NeuroScience. In *2006 6th IEEE-RAS International Conference on Humanoid Robots*, (pp. 182–187). ISSN: 2164-0580.
- Chevallereau, C., Bessonnet, G., Abba, G., & Aoustin, Y. (Eds.). (2009). *Kinematic and Dynamic Models for Walking*, (pp. 1–126). John Wiley Sons, Ltd.
- Englsberger, J., Ott, C., Roa, M. A., Albu-Schäffer, A., & Hirzinger, G. (2011). Bipedal walking control based on Capture Point dynamics. In *2011 IEEE/RSJ International Conference on Intelligent Robots and Systems*, (pp. 4420–4427).
- Erbatur, K. & Kawamura, A. (2003). A new penalty based contact modeling and dynamics simulation method as applied to biped walking robots. In *Proc. 2003 FIRA World Congress*, (pp. 1–3).
- Feng, S., Xinjilefu, X., Atkeson, C. G., & Kim, J. (2016). Robust dynamic walking using online foot step optimization. In *2016 IEEE/RSJ International Conference on Intelligent Robots and Systems (IROS)*, (pp. 5373–5378). IEEE.
- Fujimoto, Y. & Kawamura, A. (1998). Simulation of an autonomous biped walking robot including environmental force interaction. *IEEE Robotics Automation Magazine*, 5(2), 33–42.
- Harada, K., Kajita, S., Kanehiro, F., Fujiwara, K., Kaneko, K., Yokoi, K., & Hirukawa, H. (2007). Real-Time Planning of Humanoid Robot’s Gait for Force-Controlled Manipulation. *IEEE/ASME Transactions on Mechatronics*, 12(1), 53–62.
- Harada, K., Kajita, S., Kaneko, K., & Hirukawa, H. (2003). Pushing manipulation by humanoid considering two-kinds of ZMPs. In *2003 IEEE International Conference on Robotics and Automation*, (pp. 1627–1632)., Taipei, Taiwan. IEEE.
- Harada, K., Kajita, S., Saito, H., Morisawa, M., Kanehiro, F., Fujiwara, K., Kaneko, K., & Hirukawa, H. (2005). A Humanoid Robot Carrying a Heavy Object. In *Proceedings of the 2005 IEEE International Conference on Robotics and Automation*, (pp. 1712–1717). ISSN: 1050-4729.
- Hirai, K., Hirose, M., Haikawa, Y., & Takenaka, T. (1998). The development of Honda humanoid robot. In *Proceedings. 1998 IEEE International Conference on Robotics and Automation (Cat. No.98CH36146)*, volume 2, (pp. 1321–1326 vol.2).
- Hirukawa, H. (2007). Walking biped humanoids that perform manual labour. *Philosophical Transactions of the Royal Society A: Mathematical, Physical and Engineering Sciences*, 365(1850), 65–77.
- Hof, A. L. (2008). The ‘extrapolated center of mass’ concept suggests a simple

- control of balance in walking. *Human Movement Science*, 27(1), 112–125.
- Hyon, S.-H. (2009). Compliant Terrain Adaptation for Biped Humanoids Without Measuring Ground Surface and Contact Forces. *IEEE Transactions on Robotics*, 25(1), 171–178.
- Hyon, S.-H., Hale, J. G., & Cheng, G. (2007). Full-Body Compliant Human–Humanoid Interaction: Balancing in the Presence of Unknown External Forces. *IEEE Transactions on Robotics*, 23(5), 884–898.
- Kajita, S., Kanehiro, F., Kaneko, K., Fujiwara, K., Harada, K., Yokoi, K., & Hirukawa, H. (2003). Biped walking pattern generation by using preview control of zero-moment point. In *2003 IEEE International Conference on Robotics and Automation (Cat. No.03CH37422)*, volume 2, (pp. 1620–1626 vol.2). IEEE.
- Kajita, S., Kanehiro, F., Kaneko, K., Fujiwara, K., Yokoi, K., & Hirukawa, H. (2002). A realtime pattern generator for biped walking. In *Proceedings 2002 IEEE International Conference on Robotics and Automation (Cat. No.02CH37292)*, volume 1, (pp. 31–37 vol.1).
- Kaneko, K., Harada, K., Kanehiro, F., Miyamori, G., & Akachi, K. (2008a). Humanoid robot HRP-3. In *2008 IEEE/RSJ International Conference on Intelligent Robots and Systems*, (pp. 2471–2478). ISSN: 2153-0866.
- Kaneko, K., Harada, K., Kanehiro, F., Miyamori, G., & Akachi, K. (2008b). Humanoid robot HRP-3. In *2008 IEEE/RSJ International Conference on Intelligent Robots and Systems*, (pp. 2471–2478). ISSN: 2153-0866.
- Kaneko, K., Kanehiro, F., Kajita, S., Hirukawa, H., Kawasaki, T., Hirata, M., Akachi, K., & Isozumi, T. (2004). Humanoid robot HRP-2. In *IEEE International Conference on Robotics and Automation, 2004. Proceedings. ICRA '04. 2004*, volume 2, (pp. 1083–1090 Vol.2). ISSN: 1050-4729.
- Kaneko, K., Kanehiro, F., Morisawa, M., Akachi, K., Miyamori, G., Hayashi, A., & Kanehira, N. (2011). Humanoid robot HRP-4 - Humanoid robotics platform with lightweight and slim body. In *2011 IEEE/RSJ International Conference on Intelligent Robots and Systems*, (pp. 4400–4407). ISSN: 2153-0866.
- Khatib, O. (1987). A unified approach for motion and force control of robot manipulators: The operational space formulation. *IEEE Journal on Robotics and Automation*, 3(1), 43–53.
- Lim, H.-O. & Takanishi, A. (2000). Waseda biped humanoid robots realizing human-like motion. In *6th International Workshop on Advanced Motion Control. Proceedings (Cat. No.00TH8494)*, (pp. 525–530).
- Lim, H.-o. & Takanishi, A. (2007). Biped walking robots created at Waseda University: WL and WABIAN family. *Philosophical Transactions of the Royal Society A: Mathematical, Physical and Engineering Sciences*, 365(1850), 49–64.
- Luh, J. Y. S., Walker, M. W., & Paul, R. P. C. (1980). On-Line Computational Scheme for Mechanical Manipulators. *Journal of Dynamic Systems, Measurement, and Control*, 102(2), 69–76.
- Morimoto, J., Atkeson, C. G., Endo, G., & Cheng, G. (2007). Improving humanoid locomotive performance with learnt approximated dynamics via Gaussian processes for regression. In *2007 IEEE/RSJ International Conference on Intelligent Robots and Systems*, (pp. 4234–4240). ISSN: 2153-0866.
- Nagasaki, T., Kajita, S., Yokoi, K., Kaneko, K., & Tanie, K. (2003). Running pattern

- generation and its evaluation using a realistic humanoid model. In *2003 IEEE International Conference on Robotics and Automation (Cat. No.03CH37422)*, volume 1, (pp. 1336–1342 vol.1). ISSN: 1050-4729.
- Nelson, G., Saunders, A., Neville, N., Swilling, B., Bondaryk, J., Billings, D., Lee, C., Playter, R., & Raibert, M. (2012). PETMAN: A Humanoid Robot for Testing Chemical Protective Clothing. *Journal of the Robotics Society of Japan*, *30*(4), 372–377.
- Nelson, G., Saunders, A., & Playter, R. (2019). The PETMAN and Atlas Robots at Boston Dynamics. In A. Goswami & P. Vadakkepat (Eds.), *Humanoid Robotics: A Reference* (pp. 169–186). Dordrecht: Springer Netherlands.
- Ott, C., Roa, M. A., & Hirzinger, G. (2011). Posture and balance control for biped robots based on contact force optimization. In *2011 11th IEEE-RAS International Conference on Humanoid Robots*, (pp. 26–33). IEEE.
- Pratt, J., Carff, J., Drakunov, S., & Goswami, A. (2006). Capture Point: A Step toward Humanoid Push Recovery. In *2006 6th IEEE-RAS International Conference on Humanoid Robots*, (pp. 200–207). ISSN: 2164-0580.
- Pratt, J., Chew, C.-M., Torres, A., Dilworth, P., & Pratt, G. (2001). Virtual Model Control: An Intuitive Approach for Bipedal Locomotion. *The International Journal of Robotics Research*, *20*(2), 129–143.
- Rardin, R. L. (2017). *Optimization in operations research* (Second edition ed.). Boston: Pearson.
- Sentis, L. & Khatib, O. (2005). Synthesis of whole-body behaviors through hierarchical control of behavioral primitives. *International Journal of Humanoid Robotics*, 505–518.
- Stephens, B. J. & Atkeson, C. G. (2010). Dynamic Balance Force Control for compliant humanoid robots. In *2010 IEEE/RSJ International Conference on Intelligent Robots and Systems*, (pp. 1248–1255). ISSN: 2153-0866.
- Takanishi, A. (2019). Historical Perspective of Humanoid Robot Research in Asia. In A. Goswami & P. Vadakkepat (Eds.), *Humanoid Robotics: A Reference* (pp. 35–52). Dordrecht: Springer Netherlands.
- Takanishi, A., Ishida, M., Yamazaki, Y., & Kato, I. (1985). Realization of Dynamic Walking by the Biped Walking Robot WL-10RD. (pp. 459–466).
- Vukobratović, M. & Borovac, B. (2005). Zero-moment point - thirty five years of its life. volume 1, (pp. 157–173).
- Vukobratović, M., Borovac, B., Surla, D., & Stokić, D. (1990). *Biped Locomotion*. Berlin, Heidelberg: Springer Berlin Heidelberg.
- Wieber, P.-b. (2006). Trajectory Free Linear Model Predictive Control for Stable Walking in the Presence of Strong Perturbations. In *2006 6th IEEE-RAS International Conference on Humanoid Robots*, (pp. 137–142).
- Yampolskiy, R. & Gavrilova, M. (2012). Arimetrics: Biometrics for Artificial Entities. *IEEE Robotics & Automation Magazine*, *19*(4), 48–58.
- Yu Ogura, Aikawa, H., Shimomura, K., Kondo, H., Morishima, A., Hun-ok Lim, & Takanishi, A. (2006). Development of a new humanoid robot WABIAN-2. In *Proceedings 2006 IEEE International Conference on Robotics and Automation, 2006. ICRA 2006.*, (pp. 76–81)., Orlando, FL, USA. IEEE.